

METHODOLOGY

Open Access



Standardized Pre-clinical Surgical Animal Model Protocol to Investigate the Cellular and Molecular Mechanisms of Ischemic Flap Healing

Edita Aksamitiene^{1,2}, Ryan N. Heffelfinger¹, Jan B. Hoek³ and Edmund deAzevedo Pribitkin^{1,4*}

Abstract

Background Some of the most complex surgical interventions to treat trauma and cancer include the use of locoregional pedicled and free autologous tissue transfer flaps. While the techniques used for these reconstructive surgery procedures have improved over time, flap complications and even failure remain a significant clinical challenge. Animal models are useful in studying the pathophysiology of ischemic flaps, but when repeatability is a primary focus of a study, conventional in-vivo designs, where one randomized subset of animals serves as a treatment group while a second subset serves as a control, are at a disadvantage instigated by greater subject-to-subject variability. Our goal was to provide a step-by-step methodological protocol for creating an alternative standardized, more economical, and transferable pre-clinical animal research model of excisional full-thickness wound healing following a simulated autologous tissue transfer which includes the primary ischemia, reperfusion, and secondary ischemia events with the latter mimicking flap salvage procedure.

Results Unlike in the most frequently used classical unilateral McFarlane's caudally based dorsal random pattern skin flap model, in the herein described bilateral epigastric fasciocutaneous advancement flap (BEFAF) model, one flap heals under normal and a contralateral flap—under perturbed conditions or both flaps heal under conditions that vary by one within-subjects factor. We discuss the advantages and limitations of the proposed experimental approach and, as a part of model validation, provide the examples of its use in laboratory rat (*Rattus norvegicus*) axial pattern flap healing studies.

Conclusions This technically challenging but feasible reconstructive surgery model eliminates inter-subject variability, while concomitantly minimizing the number of animals needed to achieve adequate statistical power. BEFAFs may be used to investigate the spatiotemporal cellular and molecular responses to complex tissue injury, interventions simulating clinically relevant flap complications (e.g., vascular thrombosis) as well as prophylactic, therapeutic or surgical treatment (e.g., flap delay) strategies in the presence or absence of confounding risk factors (e.g., substance abuse, irradiation, diabetes) or favorable wound-healing promoting activities (e.g., exercise). Detailed visual instructions in BEFAF protocol may serve as an aid for teaching medical or academic researchers basic vascular microsurgery techniques that focus on precision, tremor management and magnification.

*Correspondence:

Edmund deAzevedo Pribitkin
Edmund.Pribitkin@jefferson.edu

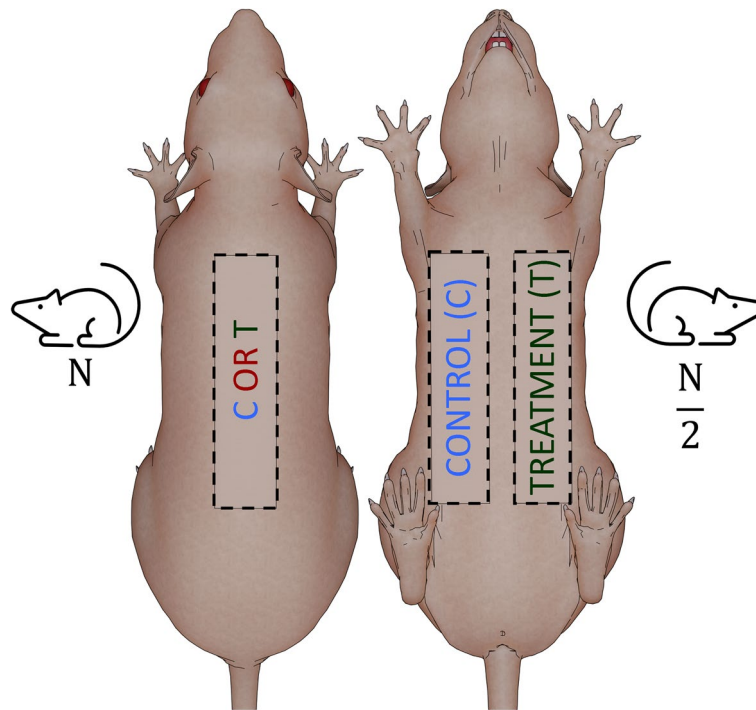
Full list of author information is available at the end of the article



© The Author(s) 2024. **Open Access** This article is licensed under a Creative Commons Attribution 4.0 International License, which permits use, sharing, adaptation, distribution and reproduction in any medium or format, as long as you give appropriate credit to the original author(s) and the source, provide a link to the Creative Commons licence, and indicate if changes were made. The images or other third party material in this article are included in the article's Creative Commons licence, unless indicated otherwise in a credit line to the material. If material is not included in the article's Creative Commons licence and your intended use is not permitted by statutory regulation or exceeds the permitted use, you will need to obtain permission directly from the copyright holder. To view a copy of this licence, visit <http://creativecommons.org/licenses/by/4.0/>. The Creative Commons Public Domain Dedication waiver (<http://creativecommons.org/publicdomain/zero/1.0/>) applies to the data made available in this article, unless otherwise stated in a credit line to the data.

Keywords Excisional wound healing, Bilateral flap, Pedicled flap, Fasciocutaneous flap, Superficial inferior epigastric vessels, Axial pattern flap survival, Primary ischemia, Reperfusion injury, Secondary ischemia, Autologous tissue transfer

Graphical Abstract



Background

Many trauma, oncological malignant or benign tumor resection and other developed soft tissue defect (e.g., arterial or venous ulcers, pressure sores, hernia, necrotic skin infections) cases require immediate or planned surgical intervention using flaps. Flaps are classified based on their [a] tissue composition (e.g., cutaneous, fasciocutaneous, myocutaneous, osteomusculocutaneous), [b] location (e.g., local, regional, distant); [c] arrangement of blood supply; [d] configuration and [e] the method of transfer onto the wound [1, 2]. For instance, a microvascular free flap is elevated from an uninjured donor site, fully detached, and transferred to the remote recipient site (Fig. 1A). Such flap is exposed to varying times of *primary ischemia* (PI) before being reconnected to recipient vessels (anastomosis). By contrast, a local or regional pedicled flap remains attached at the harvest site by vascular subcutaneous tissue base known as a *pedicle*. During surgery, such a pedicled flap can be rotated a certain number of degrees around a

pivotal point located at the base of the flap to reach and cover an adjacent, nearby, or distant recipient area (rotational, transposition or interpolated flaps) (Fig. 1B). In other cases, a pedicled flap is simply moved over a local or distant defect without altering the plane of the pedicle (advancement flaps) (Fig. 1C) [3, 4].

Preclinical wound healing models distinguish among incisional and excisional wounds, flaps, and skin grafts. Unlike small incisional and excisional wounds, flaps do not heal by contraction. A graft has no intact blood supply and therefore relies entirely on diffusion of nutrients and a number of new blood vessels derived from the recipient wound bed. By contrast, a flap contains native blood supply. In an *axial pattern flap* (APF) the blood is delivered via a dominant and well-defined cutaneous artery that is often accompanied by a large-scale vein. In a *random pattern flap* (RPF), the blood is supplied via an unnamed subdermal perforator plexus. Due to their increased length and more robust inherent blood supply, APFs are ideally suited for reconstruction of large soft tissue defects that are beyond the reach of shorter and

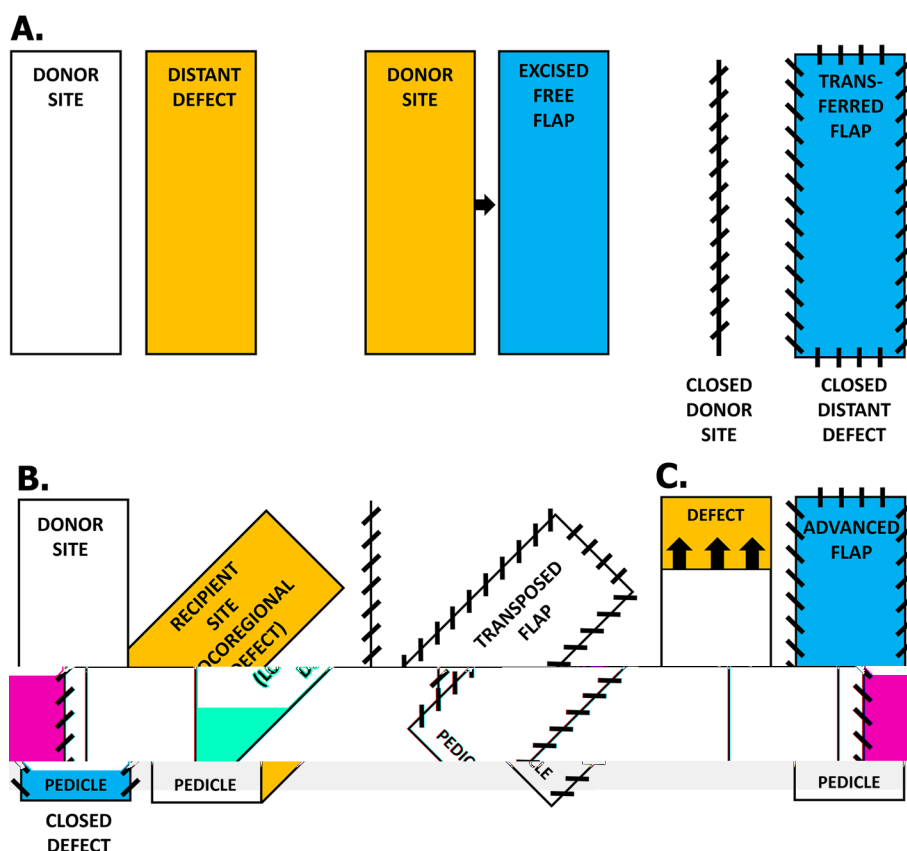


Fig. 1 Example of surgical flap classification based on the method of tissue transfer onto the soft tissue defect (wound). Principles of creating the microvascular free flap (A), single-pedicated transposition flap (B) or single-pedicated advancement flap (C) during reconstructive surgery. Diagonal lines represent running sutures

less predictable RPFs. Nevertheless, the survival pattern of APFs is typically based on the integrity and extent of their main feeding and draining vessel(s). Thus, a distal portion (the very tip) of the APF that exceeds the distance of the underlying longitudinal artery may behave as a graft or an RPF: after a reconstructive surgery, these distal tissues stay deprived of oxygen (ischemic) significantly longer depending on the rate of reperfusion, angiosome formations and extent of neovascularization, which appears later in wound healing process, but in most animal models – typically within a week [5–7]. To a certain degree, naturally occurring hypoxia (the lack of oxygen) will stimulate the APF-infiltrated and APF-residing cells to release pro-inflammatory cytokines and angiogenic factors contributing to the inosculation (connection of pre-existing vessels to the vessels of recipient wound bed and sidewalls) and angiogenesis (the ingrowth of new vessels). But if hypoxia persists, sustained inflammation combined with local accumulation of reactive oxygen species and lactic acid buildup will lower the intracellular pH and cause severe DNA damage. As a result of extensive apoptosis-related protein

activation, depleted bioenergetic resources such as nicotinamide adenine dinucleotide (NAD+) would trigger massive cell death and, subsequently, devitalized tissue breakdown (necrosis) [8–10].

Despite recent advances in surgical techniques and post-operative monitoring that contribute to a high (~85–95%) flap success rate [11–14], complications associated with vascular compromise and ischemic partial- or full-thickness necrosis remain a significant clinical problem, particularly in angiopathic, obese, post-irradiated, actively smoking and/or alcohol-abusing individuals [15–24]. In addition to inducing debilitating patient stress, flap failures inordinately contribute to health care costs due to prolonged hospitalization, readmission and revision surgery [25]. The success rate of salvaged microvascular free flaps ranges from 28% to over 90%, depending on the type of the flap being used, the etiology of its failure, the timing of its salvage and the overall experience of medical center surgeons and staff [26–28].

Experimental translational plastic and reconstructive surgery research animal models of complex full-thickness wound closure and healing using RPFs or APFs are

indispensable tools in studying physiological and pathophysiological responses to acute intermittent hypoxia and ischemic tissue injury [29]. These models provide insights into a spatiotemporally regulated activation machinery of integrated signaling pathways that induce transcription of genes controlling the survival, motility, proliferation, and differentiation of multiple functionally distinct cell populations. Under the influence of diverse endogenous stimuli these locally residing, or newly arrived wounded cells are capable of either maintaining or ceasing inflammation. Some of them promote vascularization through angiogenesis and lymphangiogenesis, change hemodynamics and induce tissue remodeling. A complete understanding of each physical and biological facet of the reparative ladder resulting in a fully recovered flap and completely closed wound is essential to predicting the clinical outcomes of the reconstructive surgery.

Many preclinical research animal wound healing models are primarily designed to investigate tissue ability to progress through different phases/stages of wound healing under unperturbed or minimally perturbed (control/sham) and experimental “treatment” conditions. The latter includes irradiation [30], photodynamic therapy [31], treatment with pharmacological agents [32–34], recombinant peptides [35], plasmid DNA or siRNA compounds [36], synthetic or natural products [37, 38] etc. Sometimes the investigators aim to mimic severe medical complications (e.g., vascular thrombosis, edema, ulcerative and infected wounds) [39] or reproduce well-known comorbidities (e.g., obesity, diabetes, ageing, smoking, alcohol intake etc.) [40–42] or stimulatory responses (e.g. exercise) [43]. Different routes and/or regimen of single or combined drug administration [44, 45], ischemic preconditioning [46, 47], delaying [48] and numerous perioperative flap treatment or handling strategies [49–53] have been evaluated for their efficacy at reducing the risk of compound flap loss. However, in all *conventional* experimental studies one randomized animal group typically serves as a control, while another group undergoes the desired treatment(s). The results obtained from such studies suffer from reduced statistical power due to high subject-to-subject variability. Pre-surgical fluctuations in baseline levels of activated proteins/genes and circulating factors may mask the moderate and less robust effects of chosen treatment(s), especially if it is applied directly onto the flap. Thus, to achieve stronger statistical power, a larger number of animals must be used.

Here we present a detailed experimental protocol to develop a standardized, versatile, scalable, transferable, and reproducible full-thickness wound closure and healing model, which simulates an actual clinical procedure of autologous free tissue transfer and is based on a *bilateral flap*. In this modified surgical pre-clinical animal

model, a treated or perturbed ventral flap is paired with a contralateral control ventral flap on the same animal which heals under similar physiological or pathological conditions. Significantly greater control for between-animal variability is obtained while sacrificing fewer animals. The presented method is a *fusion* of three clinically relevant experimental techniques: pedicled APF advancement, free microvascular flap surgery and flap salvage. We provide step-by-step guided visual instructions on creating the *bilateral epigastric fasciocutaneous advancement flap* (BEFAF) model for the intermittent collection of tissue biopsies and a final evaluation of ischemically-challenged flap survival at one designated endpoint in laboratory rat (*Rattus norvegicus*), because training with live rats is considered the gold standard in the current microsurgical training [54]. The chosen rats may be any desired strain, sex, age, and weight – due to the differences in skin anatomy and ischemic tolerance (female vs male), or wound healing efficacy (young vs old)—they all come with different advantages. These animals may be housed under routine or specialized husbandry conditions and fed ad libitum or a specialized (e.g., alcohol-containing) diet. They may be randomly selected and divided into two or more experimental groups receiving any control or experimental treatment prior to flap raising surgery. We overview data collection and analysis strategies showing representative micrographs of flap tissue sections obtained from male or female animals subjected to identical or similar surgical procedures. Finally, we discuss potential model applications, limitations, and anticipated challenges.

Materials and Methods

Design of BEFAF Model

In the current adaptation of the APF model to reconstruct an abdominal wound, we employ a bilateral epigastric fasciocutaneous advancement flap (BEFAF), which is based on two ventral APFs supplied by the caudal superficial inferior epigastric artery (SIEA) and drained by superficial inferior epigastric vein (SIEV). SIEA and SIEV branch from the femoral artery/vein in the left and right groin regions. In clinical practice, SIEA-based epigastric flaps are used either as unipedicled or bipedicled advancement or transposition flaps to cover ipsilateral or contralateral wounds on the abdomen, perineum or hindlimbs, or as free flaps to repair facial or distant breast defects as a result of trauma, burns, tumor resection or infection [55–63].

First, we create a full-thickness soft tissue defect in the upper abdomen region: a piece of fasciocutaneous tissue measuring between 0.5×3 cm and 1×3 cm is excised from the top portion of a flap prior to its elevation. Due to the absence of extensive physical manipulation, the

excised tissue thus reflects the basal activation, expression and/or spatial distribution patterns of genes, microRNAs, and proteins. In routine histological tissue sample analysis, it represents morphologically normal unwounded skin (control). The qualitative features as well as quantitative measures obtained at this baseline (0 h) can be readily compared to the ones obtained within the proximal (P), middle (M) and distal (D) flap segments at specific time points following an excisional and ischemic injury. Taking a second biopsy from the D segment of the raised flap prior to its advancement and final wound closure results in a *fully advanced* APF with a clinically recommended 3:1 or 2.5:1 height to width ratio, although these guidelines are not absolute. If the combined excised tissue area is insufficient for analysis (less than 1.5×3 cm), then a third biopsy may be acquired at any intermediate time point via minor survival surgery. The degree of tissue necrosis and overall survival, expressed as flap viability percentage (FV%), is evaluated by *digital planimetric analysis* using digital photographs of ready-to-be harvested flaps at any designated postoperative day (POD) [51]. These endpoints typically represent the peaks of major wound healing stages: inflammation (POD1 to POD3), proliferation (POD 5 to POD 7) and short-term or long-term remodeling (POD 9 to 14 and beyond). The *rate of flap healing/failure* may be calculated through this sequential planimetric analysis. The most common variables for comparative BEFAF analysis are listed in Table 1.

Importantly, with this BEFAF model, one may fully recreate *microvascular free flap surgery*. One or both flaps can be entirely detached from their primary blood supply followed by end-to-patch anastomosis. Alternatively, atraumatic vascular clamps may be gently applied onto both feeding and outflow vessels in one or both flaps for as long as it would presumably take the surgeon to separate the tissue, transfer and reconnect it to the exposed vessels of the wounded area. The global *primary ischemia* (PI) typically lasts no more than 2 h, but depending on the experimental aims, flap type and animal species used, the induced PI time may be tailored to be either shorter or longer. Furthermore, the BEFAF model presents an opportunity to examine the effects of acute or late *secondary ischemia* (SI). SI may be artificially induced by temporary closure of the SIEA, SIEV or both vessels after a certain *primary reperfusion* (REP₁) period following global PI. Such experimental design directly and selectively mimics *arterial* (AO), *venous* (VO) or *mixed arterio-venous* (AVO) occlusion. These types of vascular complications most frequently occur within first 72 h after free tissue transfer and are a major contributor to flap loss [64–67]. In this BEFAF model, flap relief from the SI would simulate a clinical *flap re-exploration and*

Table 1 Suggested pre-operative or perioperative flap handling or treatment conditions for the comparative short-, intermediate- or long-term whole flap or segmental gene or protein expression, cell signaling, extracellular vesicle release, neovascularization, tissue survival and other analyses within one subject

Left flap	Right flap
Control naïve flap (raised and placed down)	Ischemic flap (e.g., 2 h of PI)
Control naïve flap (raised and placed down)	Flap with inserted sterile silicone sheet
Control naïve flap (raised and placed down) APF	Permanently ligated artery, vein, or both ^a RPF
Global PI (e.g., 2 h)	Global PI (e.g., 6 h)
Global PI (e.g., 2 h)	Global PI (e.g., 2 h)
REP ₁ (e.g., 4 h)	REP ₁ (e.g., 12 h)
Global SI (e.g., 2 h)	Global SI (e.g., 2 h)
Global PI (e.g., 4 h)	Global PI (e.g., 4 h)
REP ₁ (e.g., 12 h)	REP ₁ (e.g., 12 h)
Global SI by AVO (e.g., 2 h)	Global SI by AVO (e.g., 6 h)
Global PI (e.g., 2 h)	Global PI (e.g., 2 h)
REP ₁ (e.g., 6 h)	REP ₁ (e.g., 6 h)
SI by AO (e.g., 2 h)	SI by VO (e.g., 2 h)
Global PI (e.g., 2 h)	Global PI (e.g., 2 h)
REP ₁ (e.g., 6 h)	REP ₁ (e.g., 6 h)
SI by AO (e.g., 2 h)	SI by AO (e.g., 6 h)
Global PI (e.g., 2 h)	Global PI (e.g., 2 h)
REP ₁ (e.g., 6 h)	REP ₁ (e.g., 6 h)
SI by VO (e.g., 1 h)	SI by VO (e.g., 3 h)
Ischemic preconditioning (e.g., 10 min × 3 times)	No ischemic preconditioning Control naïve flap (raised and placed down)
Delayed flap (e.g., 7 days)	No delay
Implantation of control PVA sponges	Implantation of drug-preloaded PVA sponges
Saline injection	Drug injection
Intradermal delivery of non-targeting control siRNA, shRNA, or antisense oligonucleotide	Intradermal delivery of targeting siRNA, shRNA, or antisense oligonucleotide
Topical treatment with control vehicle	Topical treatment with an agent of interest
No anastomosis applied	Anastomosis

Abbreviations: PI Primary ischemia, SI Secondary ischemia, AO Arterial occlusion, VO Venous occlusion; AVO Arteriovenous occlusion, REP₁ Primary reperfusion
^a flap ligation is a positive control used to estimate the maximal extent of flap failure upon complete blockade of blood flow through the main artery. This procedure turns the APF into RPF

salvage procedure. Once the congestion is alleviated, the flap would go through the *secondary reperfusion* (REP₂) and recovery period.

Both REP₁ and REP₂ are else known as reoxygenation events during which blood supply returns to the ischemic regions of the tissue. Depending on the degree of flap hypoxia and the rate of blood return, the restoration of circulation may result in mild or severe inflammation and oxidative damage through the induction of

oxidative stress rather than (or along with) restoration of normal tissue function. This phenomenon of *ischemia–reperfusion injury* (IRI) is well-known and has been widely explored mechanistically [68, 69]. The BEFAF model allows investigators to assess the tolerance of male vs female or treated vs untreated animal flaps to the selective PI and/or SI events, generating probit analysis curves and calculating the *critical ischemic time* (CIT₅₀) values when 50% of flaps become totally necrotic (Table 2) [32]. In the BEFAF surgery workflow provided below, the left-side flap is subjected to 4 h of global PI, 2 h of REP₁ and 4 h SI by VO, while right-side flap is subjected to 4 h of global PI, 2 h of REP₁ and 4 h of SI by AO.

One additional advantage of using the BEFAF model is that during an inflammatory phase of wound healing such flap produces copious amounts of *wound exudate* (WE). This growth factor-, cytokine-, chemokine-, metalloproteinase- and extracellular vesicle (EV)-enriched fluid freely travels from the caudal to the cranial regions of ventral flaps facilitating the diffusion of vital healing factors that in turn promote cell migration across the wound bed, cell proliferation,

metabolism and aid the autolysis of damaged tissues [70]. The flap can be pre-opened for the manual collection of WE into a sterile 1000 µL pipette tip after a flap is gently squeezed at the base. But more conveniently, one or more sterile polyvinyl alcohol (PVA) sponges can be implanted underneath the flap to absorb the WE over time [71]. Control sponges may be subcutaneously placed in the midline between the left and right flap or outside of each flap further away from the wound. The sponges are eventually removed by opening the pockets in the respective portion(s) of the flap(s) through minor survival and/or non-survival (endpoint) surgery. Alternatively, the PVA implants may be preloaded or continuously injected with a control vehicle or an experimental treatment solution to evaluate its impact on the migratory properties of different wound-bed cell populations, rate of granulation tissue (GT) formation and its health (thickness, vascularity), lymphangiogenesis as well as deposition of extracellular matrix and collagen fibers [72–75].

The materials required for an optional WE extraction from implanted PVA sponges and an optional isolation of

Table 2 Experimental research animal model designs for estimating the critical primary and secondary ischemia times for single-pedicled flaps in male and female subjects at 95% power and planned minimum 3 h time gap between two anesthesia events on the same subject

Animal number per group excluding attrition		Left flap	Right flap
Study Design A			
Group A	Group B		
7 female	7 male	No PI	Ligation ^a
7 female	7 male	PI for 2 h	PI for 8 h
7 female	7 male	PI for 4 h	PI for 10 h
7 female	7 male	PI for 6 h	PI for 12 h
N=28	N=28	n=7, r=1 per group	n=7, r=1 per group
Study Design B			
7 female	7 male	No PI	PI for 2 h
7 female	7 male	PI for 2 h, REP for 6 h, SI for 1 h	PI for 2 h, REP for 6 h, SI for 4 h
7 female	7 male	PI for 2 h, REP for 6 h, SI for 2 h	PI for 2 h, REP for 6 h, SI for 6 h
N=21	N=21	n=7, r=1 per group	n=7, r=1 per group
Study Design C			
7 female	7 male	No PI	PI for 2 h
7 female	7 male	PI for 2 h, REP for 12 h, SI for 1 h	PI for 2 h, REP for 12 h, SI for 5 h
7 female	7 male	PI for 2 h, REP for 12 h, SI for 3 h	PI for 2 h, REP for 12 h, SI for 7 h
N=21	N=21	n=7, r=1 per group	n=7, r=1 per group
Study Design D			
7 female	7 male	No PI	PI for 2 h
7 female	7 male	PI for 2 h, REP for 24 h, SI for 2 h	PI for 2 h, REP for 24 h, SI for 8 h
7 female	7 male	PI for 2 h, REP for 24 h, SI for 4 h	PI for 2 h, REP for 24 h, SI for 10 h
7 female	7 male	PI for 2 h, REP for 24 h, SI for 6 h	PI for 2 h, REP for 24 h, SI for 12 h
N=28	N=28	n=7, r=1 per group	n=7, r=1 per group

^a vessel ligation is a positive control used to estimate the maximal extent of flap failure upon complete blockade of blood flow through the main artery

tissue-derived proteins, nucleic acids (mRNA), or EVs are provided in the Additional File 2.

Animals

Male and female 10–18-month-old retired-breeder Sprague–Dawley (SD) rats (Charles River Laboratories, Malvern, PA and Envigo, Indianapolis, IN) with an average weight of 310 g and 570 g or male 10-month-old retired-breeder Lewis rats with an average weight of 542 g (Envigo, Indianapolis, IN) were used in this study. Rats of same sex were acclimated at least 7 days prior to surgery under standard laboratory conditions (temperature $21\text{ }^{\circ}\text{C} \pm 2\text{ }^{\circ}\text{C}$, humidity $55\% \pm 10\%$, 12:12 h light–dark-cycle). Due to the weight ($>500\text{ g}$) and retired breeder status males were housed singly. Females were housed in tandem. Food and water were provided in a standard manner. Some animals received liquid ethanol-supplemented diet. We show representative photos of experimental male or female animals.

General Laboratory Equipment and Materials for the Surgeon

This procedure used standard ACS $\geq 95\%$ purity or molecular biology grade laboratory reagents/chemicals as well as standard veterinary surgery and microsurgery equipment/tools. In some instances, the shortened links to the randomly selected vendors that can supply specific surgical instruments or reagents used in this study are provided next to the item.

1. Personal protective equipment (PPE): surgical gown, ear loop face mask, hair cap, shoe covers, sterile surgical gloves, non-sterile gloves, safety glasses.
2. Stainless steel instrument tray with flap cover – for autoclaving and storage of surgical instruments
3. Stainless steel Grafco Flat Type instrument tray – for placing the surgical items during the procedure (Additional File 2, Fig. S1)
4. Sharps disposal container – for disposal of needles and syringes
5. Biohazard disposal container and biohazard bags – for safe disposal of biohazardous trash, including pipette tips.
6. Countdown timers
7. Digital camera with macro-view function

Optional:

8. Magnifying spectacles or loupes (2.5–3 \times , depending on the eyesight of the surgeon) with/without illumination or separate LED headlamp (>500 lumens).

Materials for Animal Preparation for the Surgery and Flap Design

1. Single or dual-channel anesthesia system with gas vaporizer, inlet flowmeter, charcoal filters, high pressure oxygen hose, oxygen regulator, and low-profile anesthesia masks adapted for rodents.
2. Small-animal scales
3. Secure animal transportation cart
4. Small animal heating pad
5. Handheld hair clipper and/or trimmer (e.g., WAHL for Home Pet).
6. Ophthalmic veterinary ointment (e.g., Puralube).
7. Betadine (10% povidone iodine) antiseptic solution.
8. Isoflurane inhalant anesthetic for veterinary use (USP)
9. Sterile non-woven or gauze sponges (e.g., Dermacea 4" \times 4", 6-Ply by Covidien, #441405)
10. Disposable surgical under pads:
 - X-large 30" \times 36" Wings Ultra by Covidien.
 - Small 17" \times 24" or medium 23" \times 24" Dri-Sorb by Attends.
11. C-fold paper towels (e.g., Kleenex)
12. Sanitizing 70% ethanol spray
13. Sterile disposable skin marking pen with ruler (Viscot, #1422SRL9-100)
14. 1:3 or 1:2.5 ratio flap design template made from sturdy card-paper with extra 1–2 cm in length if distal biopsy collection is intended.

Materials for Major or Minor Survival Surgery

1. Pre-operative analgesic (opioids such as sustained release buprenorphine hydrochloride are typically obtained from LAS veterinarian staff). Otherwise, take a new sterile 1 ml syringe, slowly draw in analgesic solution into the syringe. Point the syringe upward to bring any air bubbles to the top of the needle. Plunge the syringe slowly to expel any air until only liquid expels from the syringe. Double check volume, place the needle cap and set a syringe aside.
2. Sterile Dulbecco's Phosphate-Buffered Saline (DPBS) (Cytiva, #SH30028.02) or HyClone™ Hank's Balanced Salt Solution (HBSS) without calcium, magnesium, and phenol red (Cytiva, #SH30588.01) – for irrigation of raised flaps while maintaining cell tonicity and viability.

3. 1% Lidocaine HCl—for topical irrigation of pedicle to prevent or reduce traumatic vasospasm(s). Prepare

4. Fine-tip histology marker and LN₂-proof cryo-marker (e.g., Dual-point UltraCruz, Santa Cruz Biotechnologies, # sc-360977)
5. -80°C freezer – for long-term tissue and sample storage.
6. Animal euthanasia cart with CO₂ gas tank supply
7. Small biohazardous waste bags or specified animal carcass disposal bags

Optional: Sterile Disposable McKesson Biopsy Punches (available in 2–10 mm sizes).

Tissue Preparation for Histology

1. UnisetTM 1-chamber histology embedding/processing cassettes with 1 mm openings (Ted Pella)—for smaller size and leaner specimens:
 - Outside dimensions: 28.5×41×6.7 mm (1.12"×1.61"×0.26").
 - Inside dimensions: 26×30 x 5 mm (1.02"×1.18"×0.2").
2. MacrosetteTM 1-chamber histology embedding/processing cassettes with 1 mm openings (Ted Pella)—for thicker specimens
3. MicromeshTM 4-compartment biopsy cassettes – for excised pedicles
4. Cassette marking histology pen (e.g., Statmark by StatLab)
5. 90 ml containers with prefilled 10% Neutral Phosphate-Buffered Formalin (pH 7.2±0.5; vials) (e.g., StatLab, # NB0345)
6. 1X PBS buffer without magnesium and calcium—for cassette washing after fixation. Store at RT.
7. 70% Ethanol solution – for cassette storage until analysis at +4°C.
8. Large glass staining dishes.
9. Stains of interest, e.g., Masson's Trichrome (MT) and Hematoxylin & Eosin (H&E).
10. Classical histology lab equipment if not using Core Histology facility.

Experimental Animal Preparation for Survival Surgery

To reduce the time of animal exposure to anesthesia during the major survival surgery, and to minimize the risk of overlapping PI or SI time between the sequentially operated animals, the animals are shaved 16–24 h prior to flap raising procedure:

1. The heating pad is set for 122°F (50 °C) and covered with two surgical underpads.
2. The anesthesia machines is turned on to prefill the padded rodent sedation chamber with 4–5% induction isoflurane gas.
3. The animal is placed in the chamber and kept there for up to 4 min.
4. 3% isoflurane flow is then redirected into the nose cone attached to the anesthesia machine.
5. The sedated rat is removed from the chamber and placed onto the heating pad in a prone position.
6. The lubricate ointment is generously applied onto animal's eyes.
7. The rat is placed back into a supine position and its fur is shaved until the nude skin is exposed.
8. The top surgical pad containing shaved fur is removed.
9. Shaved skin areas are wiped with betadine solution, which is copiously applied onto a non-woven sponge.
10. Animal weight is recorded in the post-operative animal monitoring sheet (POAMS) (see Additional File 1).
11. The animal is returned to the cage and monitored until awakened.

NOTE: If less than three consecutive animal surgeries are anticipated one after the other within the same day, animal shaving should be performed on the same day as major survival surgery without an animal being awakened. With experience and proper equipment, animal fur clipping takes less than 12 min. Chemical hair removal creams such as "Nair" are not recommended as they may affect both baseline and injury-inducible biological molecule distribution and/or expression patterns, cause skin irritation or allergic reaction.

Major Survival Surgery

As a visual aid, we used black non-absorbable silk sutures in every but the final suturing step. These sutures must be replaced with non-absorbable sutures where and when indicated in the protocol.

Preparation

1. Appropriate PPE is donned by the surgeon.
2. The HDPE tubes, 10% formalin-prefilled containers and histology cassettes are labeled for appropriate specimen.
3. The vascular clamps, that are being stored in enzymatic solution, are removed, washed with distilled water, and then placed in an Eppendorf tube containing 70% alcohol.

4. The hot glass bead sterilizer is turned on to preheat.
 5. The heating pad is set to reach 122°F (50 °C). It is covered with four surgical underpads: 1 extra-large and 3 medium or small.
 6. If an optional PVA sponge implantation is desired, then two sterile 9 mm × 15 mm ear wicks are placed onto 100 × 20 mm tissue culture dish prefilled with sterile PBS. These wicks are then cut into three pieces per each using a disposable scalpel. The lid of tissue dish is closed to prevent the PVA sponges from drying.
 7. The dose of analgesic agent is prepared for each individual animal based on the recorded animal weight (for example, our rats received 1.0–1.2 mg/kg of Buprenorphine-HCl-SR formulation subcutaneously (sc)).
 8. Dewar flask is prefilled with liquid nitrogen (LN₂).
 9. Isoflurane and oxygen tank levels are checked, and the proper amount of isoflurane is added to the gas anesthesia machine chamber before the experiment if needed. The anesthesia machine is turned on to prefill the padded rat sedation chamber with 4–5% isoflurane gas.
1. The animal is placed into the anesthetic sedation chamber and kept there for up to 4 min.
 2. 3% isoflurane flow is redirected into the nose cone attached to the anesthesia machine.
 3. The sedated rat is removed from the chamber and placed onto the heating pad in a prone position.
 4. Animal's eyes are lubricated by applying the ointment, and analgesia is injected sc.
 5. The animal is turned back to the supine position. The use of medical tape for animal stabilization during the flap design procedure is not recommended, as the animal skin should be in the most natural and relaxed condition.
 6. Flap boundaries are identified by applying a pre-cut cardboard 9.5 × 3 cm flap design template and drawing a single dotted line with a skin marker. After removing the template, a second dotted line is drawn above the first just a few millimeters apart. Finally, a solid line is drawn through the inner dots as shown in Fig. 2A.
 7. Flap areas that will be used for the excisional biopsies are then marked. In the example provided herein we defined four 1 × 3 cm biopsy areas:
 - A) B₀ – baseline.
 - B) B_{PI} – to be excised after the end of global primary ischemia (PI) and prior to reperfusion.
 - C) B_{VO} – to be excised after the end of secondary venous ischemia.
 - D) B_{AO} – to be excised after the end of secondary arterial ischemia (Fig. 2A).

Flap Design

To prevent tension-associated flap failure, the BEFAF model allows taking only a limited number of tissue biopsies from the distal clinically most relevant part of the flap prone to failure. Additional biopsies, if required, may be obtained from the regions that lie along and close to the suture line, however, such biopsies introduce an additional variable. Therefore, in flap survival studies, no interference other than collection of biopsies from the distal portion of the flap throughout the entire course of experiment is strongly recommended. For a flap with initial measurements of 9.5 × 2.5 cm or 9.5 × 3 cm, the maximal flap advancement is 2 cm, which leaves a healing area of 3:1 or 2.5:1 length to width ratio. Consequently, one can obtain two 1 cm or four 0.5 cm wide biopsies from each flap. The 1 × 3 cm tissue strip is big enough to be divided into three or four segments for postoperative imaging or biochemical analysis, especially if sample pooling is allowed. On the other hand, such long and wide initial flap can be created only in adult, over 500 g rats. These are usually males. Female rats rarely exceed 350 g of weight. Therefore, for smaller animals, flap dimensions should be downsized appropriately, keeping in mind that a healing flap shrinks approximately 0.5 – 1 cm, which may partially limit animal movements and cause distress.

Assuming the morphology and cellular activities in left and right side are similar under identical conditions, we aim to take B₀ and B_{PI} biopsy only from one of the flaps. NOTE: in an alternative experimental design, one can excise four 1 × 1.5 cm biopsies out of each flap that would include in a dedicated B₀, B_{PI} and B_{VO} or B_{AO} sample plus one extra sample, e.g., B_{REP1}—to be taken after the end of primary reperfusion prior to SI. However, the created gap resulting from partial tissue excision would need to be protected by gauze during intermediate incubation periods prior to final wound closure (see Additional File 2, Fig. S2).

Flap Raising

The tissues being raised in this protocol consist of skin and fascia but exclude muscle. Depending on the research objective, other types of composite flaps (e.g. myocutaneous flap) could be raised instead, but they may require another suturing approach, and due to different sensitivity to ischemia – adjusted PI and SI times [76, 77].

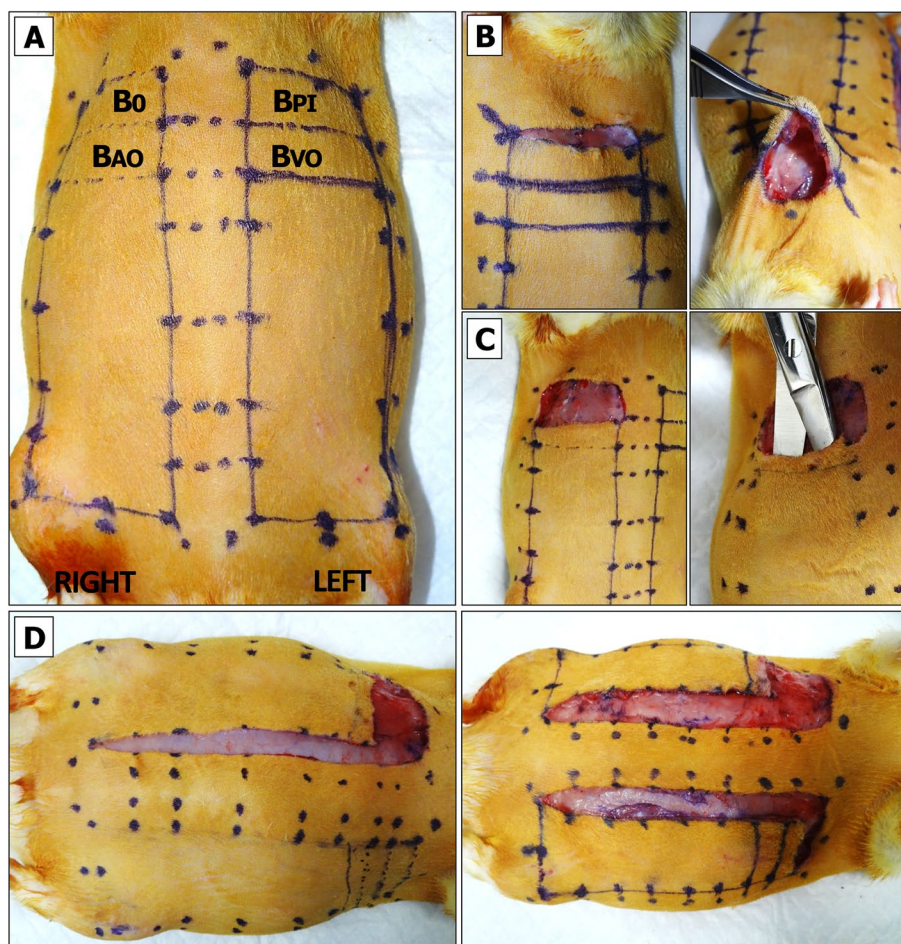


Fig. 2 Design of BEFAF. **A** Contours for flap elevation and biopsies. **B** Preparation of flap for baseline biopsy (B_0) excision. **C** Flap pocket after B_0 excision is used for blinded dissection and partial separation of fasciocutaneous tissue from the muscle. **D** Superficial cutting of inner flap sidewalls

1. An incision on the top of the flap is made using straight Iris Supercut scissors. The cut is deepened. A portion of biopsy area is released from the fascia using Mayo dissecting scissors (Fig. 2B).
2. The baseline (B_0) biopsy area is lifted using Adson tissue forceps. This portion of skin is then cut out using Metzenbaum-Nelson scissors (Fig. 2C, left panel).
3. For HIS/IHC, the excised specimen is divided using a straight Iris Supercut scissors. The specimen is placed into a pre-labeled histology cassette, which is submerged in 10% formalin. For long-term tissue storage, the remaining specimen pieces are placed into the pre-labeled HDPE tube, which is sealed and submerged in LN_2 .
4. After a re-entry to the existing pocket, the tissue is dissected underneath the flap by slowly moving Mayo scissors towards the pedicle (Fig. 2C, right panel). It is important not to open the scissors too wide beyond the medial boundaries of the designed flap.
5. Straight Iris Supercut or Metzenbaum-Nelson scissors are used to cut through the inner sidewall of the flap up to its end (Fig. 2D, left panel). The same is done for the opposite side (Fig. 2D, right panel). Some portions of the flap may still be attached to the underlying muscle by vascularized fascia (Fig. 3A, left panel). If so, a flap is lifted, and the fascia is cauterized so that the flap can be freed up to its base (Fig. 3A, right panel).
6. Straight Iris Supercut or Metzenbaum-Nelson scissors are used to cut through the lateral solid line of the flap roughly to its midline (Fig. 3C, left panel). From this point forward only the superficial layer of the flap should be cut through to avoid the damage of lateral branch of the SIEA (Fig. 3C, right panel). The same is done for the opposite side.

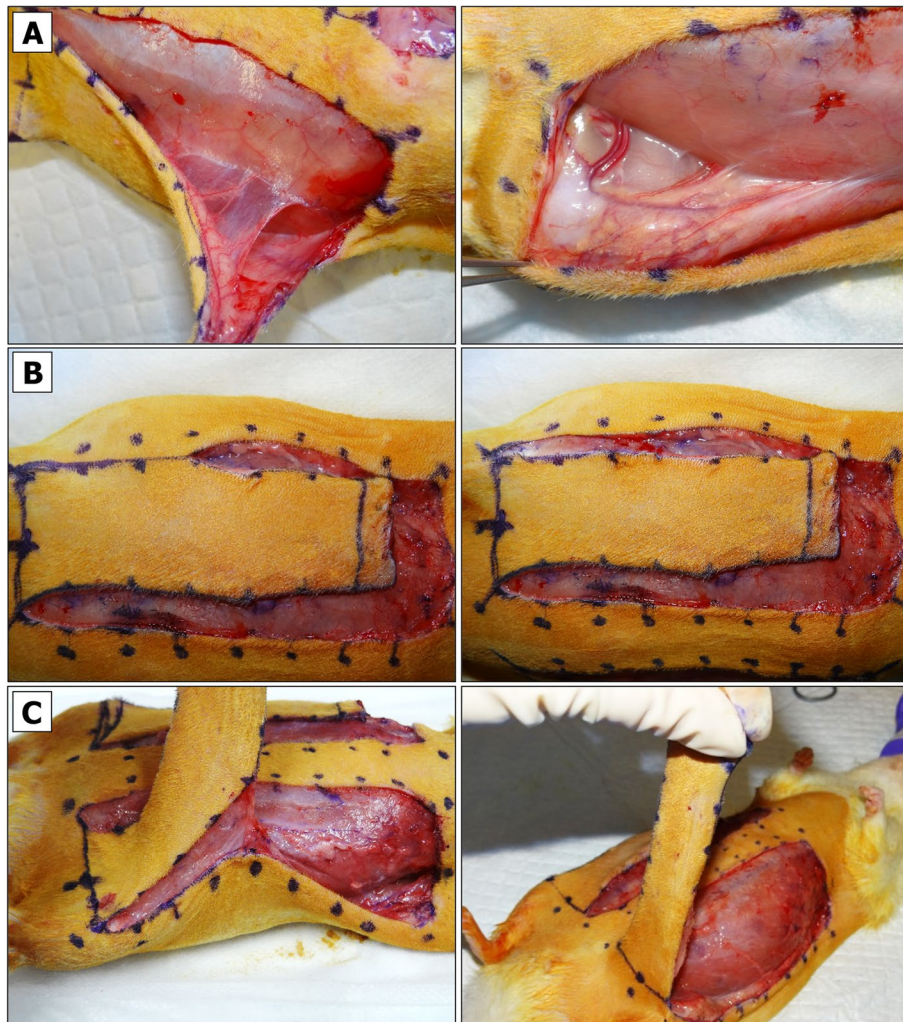


Fig. 3 Raising BEFAF. **A** Full separation of fasciocutaneous tissue from the underlying muscle. **B** Superficial cutting of outer flap sidewall to preserve the lateral branch of SIEA vessel. **C** Flap positioning for electrocautery (left panel) and flap elevation on its base post-cautery (right panel)

7. The cautery device is used to cut through the tissue of the elevated flap until its base (Fig. 3D). The same is done for the opposite side.
8. Both flaps are returned into their original horizontal position.

Physical Vessel Separation and Selective Clamping to Induce Primary Ischemia (PI)

1. The pedicle is exposed. Some rats have abundant fatty tissue obscuring a view to the emerging SIEA/SIEV bundle from femoral artery/vein. Such cases require a deeper dissection and removal of more fascia around the thigh and the vessels (Fig. 4A). Once the vessels appear clean, each flap is wrapped in sterile gauze moistened with sterile DPBS to pre-

serve them from drying and return to the original horizontal position (Fig. 4B). NOTE: to minimize variation, the temperature of DPBS should be kept constant unless the objective is to compare the viability of flaps exposed to warm or cold ischemia.

2. Isoflurane flow should be decreased to 2%.
3. Holding the tip and the center portions of the wrapped flap, a flap is positioned over the animal's thigh so that the pedicle appears in an extended position (Fig. 4C).
4. The SIEA and SIEV vessels are irrigated in 1% Lidocaine HCl solution applied dropwise.
5. At this point the vessels of the pedicle may be examined more closely. The most suitable site for physical SIEV or SIEA separation is based on vessel anatomy and the surgeon's left- or right-handedness. Vessel anatomy in male and female rats

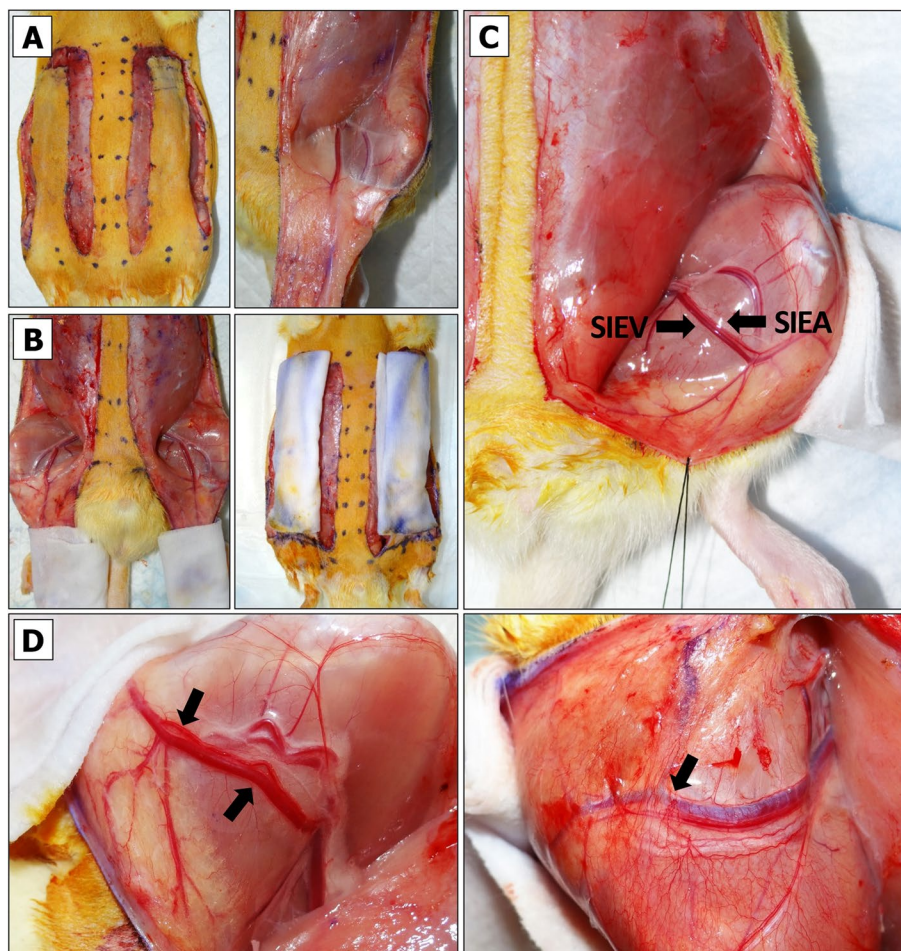


Fig. 4 Exposure of BEFAF pedicle. **A** Flaps in their original closed and opened positions. **B** Flap irrigation. **C** Exposure of left pedicle once the flap is in an extended position. **D** Representative anatomy of the pedicle in female (left panel) and male (right panel) rats. Black arrows indicate the best target points to pass a suture for the most effective and safest SIEA and SIAV vessel separation

slightly differs. In contrast to females (Fig. 4D, left panel), male SIEA may be less pronounced and run very close to SIEV without making large loops (Fig. 4D, right panel), which may pose a challenge for their separation without an aid of magnifying spectacles and LED headlight.

6. For SIEV isolation the Halsey micro needle holder scissors are used. Once the largest gap between the SIEA and SIEV before the point of SIEV bifurcation is identified (Fig. 5A), a 4–0 size needle with attached silk suture is passed between the SIEA and SIEV in a direction shown in Fig. 5B. When the needle shows on the opposite side of SIEV, the scissors are released. The needle is grabbed close to the tip and slowly pulled upwards until the suture is underneath the SIEV (Fig. 5C). **CRITICAL:** if one of the vessels gets accidentally punctured, the bleeding can be stopped by clamping, raising both vessels and ligating them with LigaClip tool. When properly ligated and cut in half, vessels should not bleed (see Additional File 2, Fig. S3A and Fig. S3B). A ligated flap may serve as a negative control for BEFAF survival. The flap (right or left) that has been ligated and the time of ligation should be immediately marked in the POAMS “Surgery notes” field (Additional File 1).
7. The suture is cut, and a loose knot is tied around the isolated vessel (Fig. 5D). **NOTE:** The 4–0 size needle should make a passage wide enough for a subsequent application of vascular clamp. It is possible to carefully widen this gap by using microscissors and lifting the attached suture loop, but it may increase the risk of vessel damage.
8. Similarly, the SIEA is separated on the opposite flap (Fig. 5E). If the SIEA forms a significant branch,

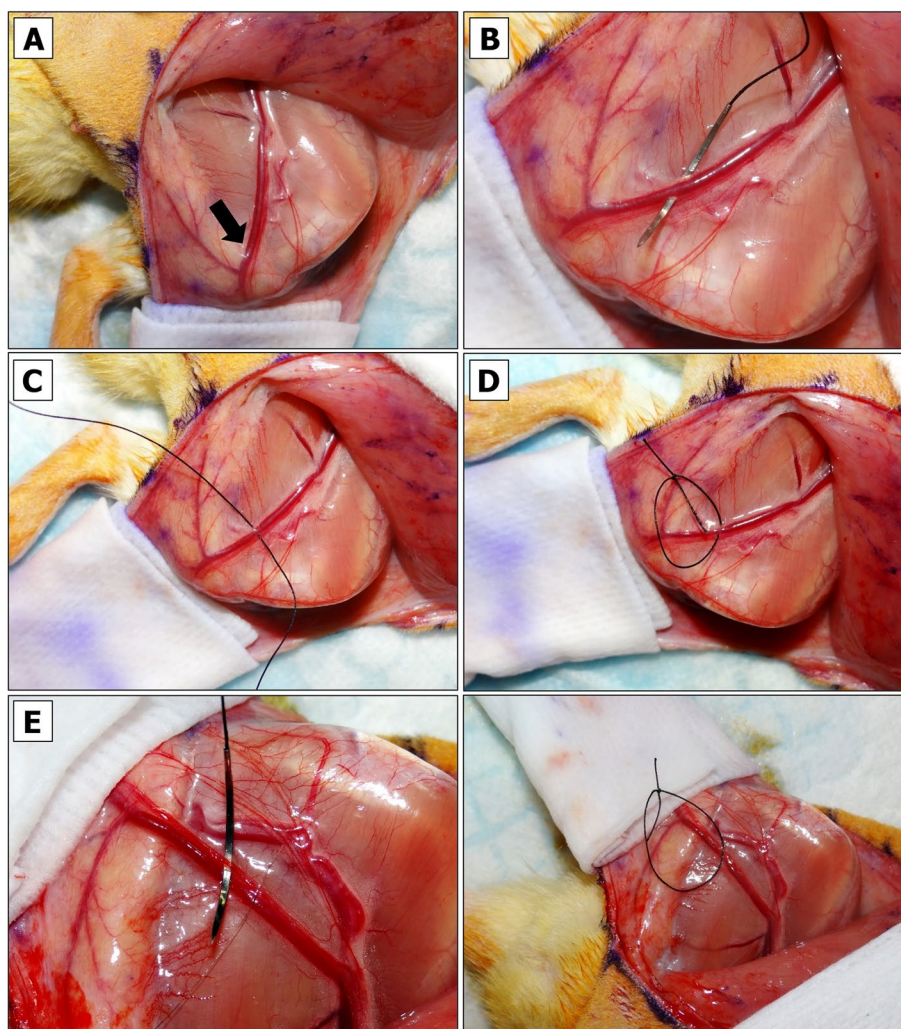


Fig. 5 Vascular separation. For the isolation of SIEV, the largest gap between SIEV and SIEA is identified when the flap is in an extended position (black arrow, **A**). The needle is inserted from the outside of vessel bundle towards the middle (**B**). Silk suture is passed (**C**), cut and tied around SIEV (**D**). SIEA is similarly separated and isolated by looping the vessel on the opposite side (**E**)

- a suture should pass right before the bifurcation point as shown in Additional File 2, Fig. S3C.
9. In the POAMS form (Additional File 1) the “Surgery Notes” field is used to indicate which vessel has been isolated by looping on the left and the right side of the animal.
 10. Slightly or fully curved smooth jaws micro forceps are used to lift fascia. Then Iris microscissors are used to make a small tunnel below the tied loop on the top and bottom of the pedicle (Fig. 6A). This passage is widened by inserting the microscissors underneath the pedicle and slowly opening them to dissect the remaining tissue (Fig. 6B). This step is repeated for the opposite side (Fig. 6C).
 11. Vascular clamp-applying forceps are used to insert one B-2 V vascular clamp onto the pedicle with an already separated SIEV (Fig. 6D). Using slightly curved microforceps, the flow below an applied clamp is gently pushed towards the femoral vein to make sure that the blood outflow from the vein is fully ceased. It is normal to see some backflow from the femoral vein. NOTE: If the venous blood surpasses the clamp, there may be too much fascia left around the vessel. If a problem persists after repositioning of a clamp, a second (smaller) clamp may be applied making sure there is no blood entrapped between the two clamps (see Additional File 2, Fig. S3D).

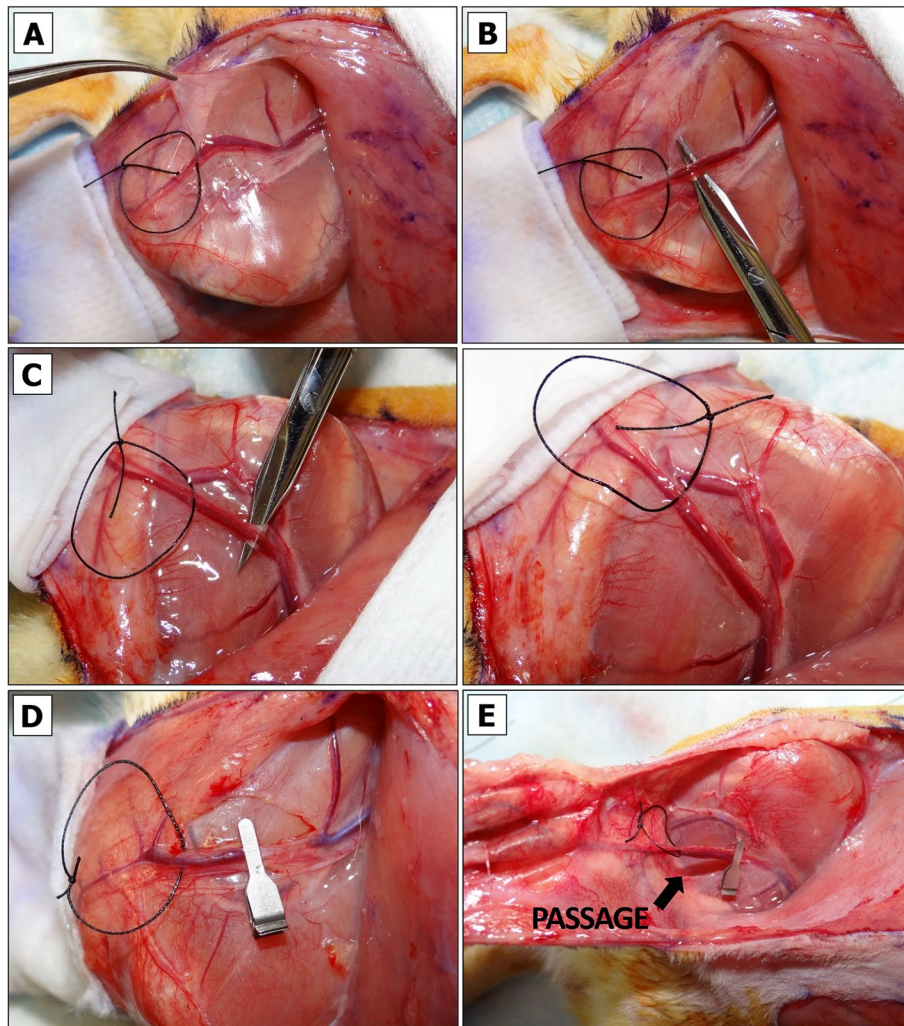


Fig. 6 Induction of primary ischemia (PI). A passage underneath each pedicle is made (A–C) large enough for passing B-2 V clamp to occlude both SIEA and SIEV vessels (D). After clamping, the passage is widened to form a ~45–60° angle with flap's base (E)

12. Once the clamp is in a proper position, a countdown timer is immediately set and started for the desired duration of the PI (e.g., 4 h).
13. Steps 11 and 12 are repeated for an opposite side. In the case of arterial occlusion, the curved microforceps should be used gently to push blood away from the site of the clamp going distally towards the flap. If the clamp is adequately applied, no influx of blood will be seen in the artery between the clamp and the curved microforceps.
14. The flap is held vertically by regular forceps, and the microscissors or fine-tip cauterly is used to widen the passage by dissecting tissue along the clamped SIEA/SIEV bundle (Fig. 6E). The angle between the isolated clamped pedicle and the flap should be ~45–60°. The same step is repeated for the opposite side.
15. Both flaps are returned to their original horizontal position. The moisture level of the gauzes that are wrapped around each flap is checked. If needed, an additional amount of sterile DPBS is applied. If the underpad is wet, it should be replaced to avoid hypothermia of the animal.
16. At this point the flap is supplied by residual microvascular plexus. To remove this feed the entire base portion of the flap is cut superficially using the Iris Supercut scissors (Fig. 7A). NOTE: this step can be omitted for local/regional pedicled advancement or rotational flaps since these do not simulate a free flap situation.
17. The tissue at the base of the flap is cauterized while holding the flap vertically (Fig. 7B). At this point, the flap becomes connected to the animal only by the clamped pedicle (Fig. 7C). CRITICAL: With-

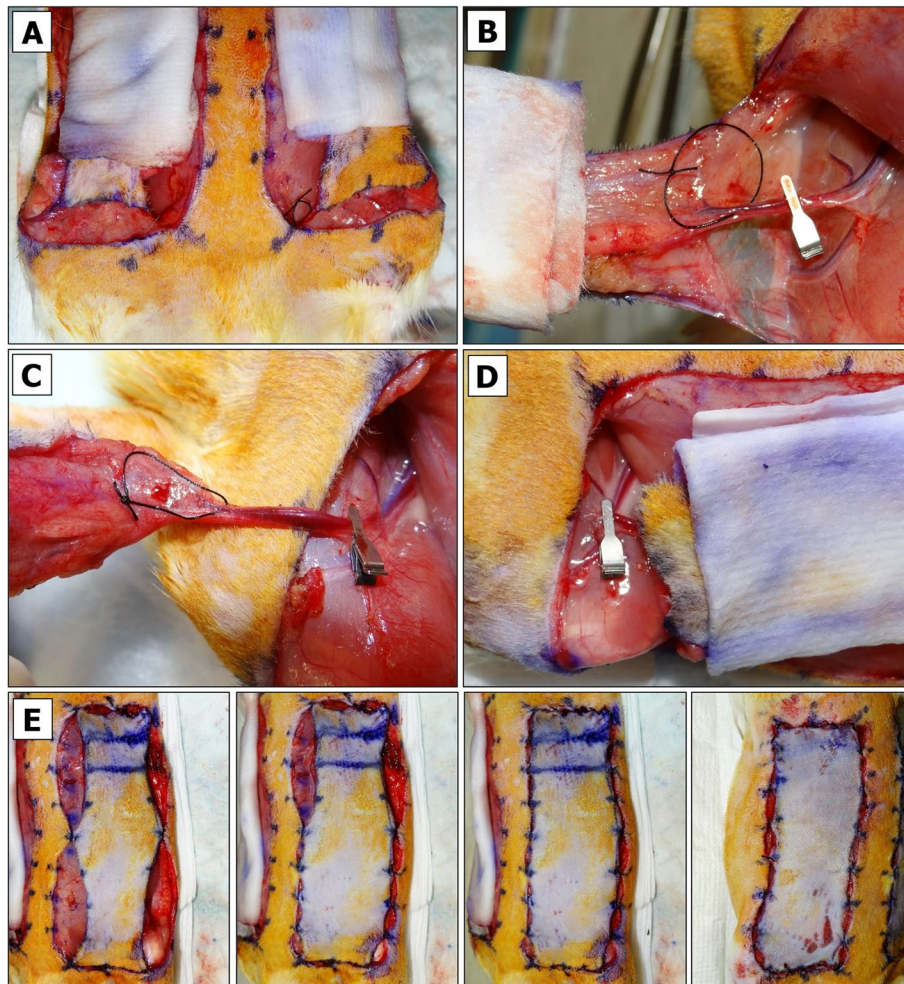


Fig. 7 Isolation of the pedicle and temporary closure of the flap. **A** top (**A**) and rear (**B**) view of superficial cut of flap's base. **C** An isolated single-pedicle flap after a complete removal of residual microvascular tissue. **D** Placement of isolated pedicle into its original position. **E** Steps for temporary left-side flap securing with non-absorbable sutures. **F** Top-view of right-side fully secured flap

out pulling the pedicle (it may cause undue strain on the vessels), the flap is returned into its original horizontal position (Fig. 7D), and this step is repeated for the opposite side.

Partial Flap Closure

1. The 2% isoflurane flow should be decreased to 1%.
2. The flaps are sutured to the wound boundaries by using buried simple-interrupted suturing technique and non-absorbable silk suture (Additional File 2, Fig. S4) in the order and directions as suggested in Additional File 2, Fig. S5.
3. First, the bottom corners of a longer flap (which did not undergo biopsy excision) are sutured, and

the same procedure is performed on a shorter flap (Additional File 2, Fig. S6). It is important to begin by suturing the base of the flap in order to minimize strain on the vascular pedicle.

4. Second, the upper corners of a longer flap are sutured followed by the center (Fig. 7E, left panel) and the remaining suturing points at the gaps (Fig. 7E, middle panel). A water-tight closure of the top and bottom parts of the flap is not necessary, but enough to prevent exposure of the clamp or vessel isolation loop and excessive accumulation of blood onto the future biopsies (Fig. 7E, right panel).
5. On the opposite side, the upper corners of a shorter flap are sutured using a non-absorbable silk suture. Finally, the center and the remaining points are sutured using an absorbable suture. NOTE: the guiding dots for suturing of this flap will not exactly

match since the flap will be slightly advanced (Fig. 7F).

6. Isoflurane flow is decreased to 0% so that the animal would receive 100% oxygen. When it starts showing the signs of awakening on the operating table, it is returned to a cage to recover.
7. The instruments are cleaned from blood and dry-sterilized using the hot bead Germinator.
8. All waste is removed, and sharps are disposed in specified containers.
9. The cage is kept in the vicinity to monitor the animal's well-being and activities more closely. If it starts extensively picking on the sutures, the Elizabethan collar should be applied.
10. Left flap is gently lifted (Fig. 8C, right panel) to remove the clamp by gripping it with the vascular clamp-applying forceps.
11. The pedicle is observed for restored blood flow (Fig. 8D). NOTE: we take note whether, upon clamp removal, there is some movement of venous blood. Small thrombi, if any, can be removed by applying a gentle sliding force with non-serrated microforceps. The vessels can be irrigated with 1% Lidocaine HCl solution applied dropwise after touching the pedicle.
12. Once the blood shows a sign of flow within the pedicle, the countdown timer is set and started for the desired primary reperfusion (REP₁) interval (e. g. 2 h).
13. Steps 9 to 13 are repeated for the right flap. Then, flap corners are sutured back to their original position using silk suture.
14. The remaining sutures on the left flap are disrupted. The top portion is reconnected to the tissue using silk suture. IMPORTANT: Then, an absorbable suture is used to connect the center and remaining parts so that both flaps are advanced equally.
15. Steps 6 to 9 from "Partial flap closure" section are repeated.

Primary Reperfusion (REP₁)

1. Fifteen minutes prior to the planned end of PI, the animal is placed into the anesthetic chamber for up to 4 min.
2. Meanwhile, two new underpads are placed onto a heating pad.
3. 3% isoflurane flow is redirected into the nose cone.
4. The sedated animal is removed from the chamber and placed onto the heating pad in a prone position. The lubricate ointment is applied onto both eyes prior to turning the animal over in a supine position.
5. Isoflurane flow is adjusted to the maintaining 2% (for larger animal) or 1% (for smaller animal).
6. The flaps are gently wiped with DPBS-moistened gauze pad to remove any aggregated blood. Then the top underpad can be removed.
7. The degree of ischemia is inspected visually in both flaps. After 2 h of PI, flap color should be significantly darker than the surrounding skin, and even more so after 4 h of PI (Fig. 8A). NOTE: if the color does not significantly differ, it may indicate that the vascular clamping was insufficient or ineffective. With the extent of usage, the gripping power of reusable clamps gets weaker, and caution must be taken to prevent the clamp from falling off the pedicle in an active animal.
8. The suture is disrupted at points #4, #5, #6, #17 and #18 from the top portion of the longer (in this example, left) flap, followed by excision of the B_{PI} biopsy (Fig. 8B).
9. The sutures are removed from points #1 and # 9 (also #3 if needed more space) at the lower midline and an inner corner of the flap base on both sides (Fig. 8C, left panel).

Secondary Ischemia (SI)

1. Fifteen minutes prior to the planned end of REP₁, the animal is anesthetized and prepared for the procedure as described previously.
2. 3% (for larger animal) or 2% (for smaller animal) isoflurane flow is redirected to the nose cone.
3. The appearance of both flaps is visually inspected to assess the approximate percent of restored blood flow. Figure 9A shows a case of efficient (~73%) reperfusion of a flap only 2 h after a designated 4 h PI time, which is well above the expected average [78].
4. The suturing points #2, #3 and #10 are disrupted at the lower sidewall and outer corners of flap base on both sides (Fig. 9B).
5. Left flap is gently lifted to inspect whether the blood flow is fully restored in the pedicle (Fig. 9C). Caution: some animals may develop spontaneous arterial or venous or mixed thrombosis after the PI (Additional File 2, Fig. S7). If a drop of heparin and 1% lidocaine does not resolve the thrombus and if the flow is not restored after a gentle push toward the groin area, the flap will be lost and should be excluded from the study. In such case, an opposite flap may be used as

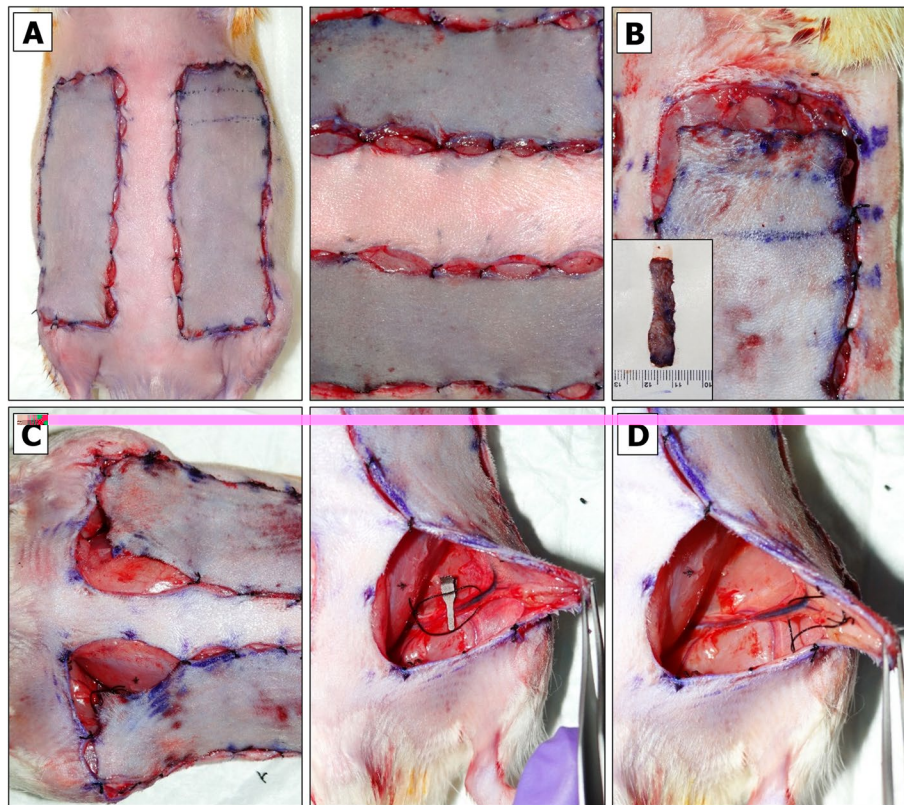


Fig. 8 Primary flap reperfusion (REP_1). **A** Macroscopic evaluation of BEFAF after 2 h (left panel) and 4 h (right panel) of PI. **B** B_{pi} biopsy excision. **C** Flap preparation for clamp removal. **D** Inspection of blood flow restoration in unclamped pedicle prior to REP_1

- 4 h PI data point or any selected SI data point without a matching pair.
6. B-1 V vascular clamp is applied onto an isolated SIEV (Fig. 9D). While applying the clamp, the suture that separates both vessels is removed. The timer is set and started for desired venous occlusion (VO) period (e. g. 4 h).
7. B-2 V vascular clamp is immediately applied onto an isolated SIEA on the opposite side. The timer is set and started for desired arterial occlusion (AO) period (e. g. 4 h).
8. The bottom of both flaps is then closed using silk sutures.
9. Steps 6 to 9 from “Partial flap closure” section are repeated.
3. The appearance of the flaps is examined to evaluate the efficacy of SI. VO flap should look significantly darker than AO flap (Fig. 9E). VO flap may be thickened by accumulated blood, which may form dark aggregates around the edges of the flap. These aggregates can be removed by flap irrigation with DPBS.
4. The sutures from the top portions of both left and right flaps are disrupted to excise the B_{VO} and B_{AO} biopsies, respectively (Fig. 9F).
5. The entire bottom of both flaps is opened widely to remove the clamps. The time of clamp removal is immediately indicated in the POAMS form to track the timing of secondary reperfusion (REP_2).
6. The pedicles are observed for the restored flow. The thrombi are removed if needed, and both vessels are irrigated in 1% Lidocaine HCl applied dropwise.

Secondary Reperfusion (REP_2)

1. Fifteen minutes prior to the planned end of AO/VO, the animal is anesthetized and prepared for the procedure as described previously.
2. 2% (for larger animal) or 1% (for smaller animal) isoflurane flow is redirected to the nose cone.

Full Flap Closure

1. The bottom of both flaps is sutured using an absorbable suture.
2. The top of naïve wound bed tissue is narrowed by suturing the upper corners together (Fig. 9G, left panel). The top corners and top middle of each

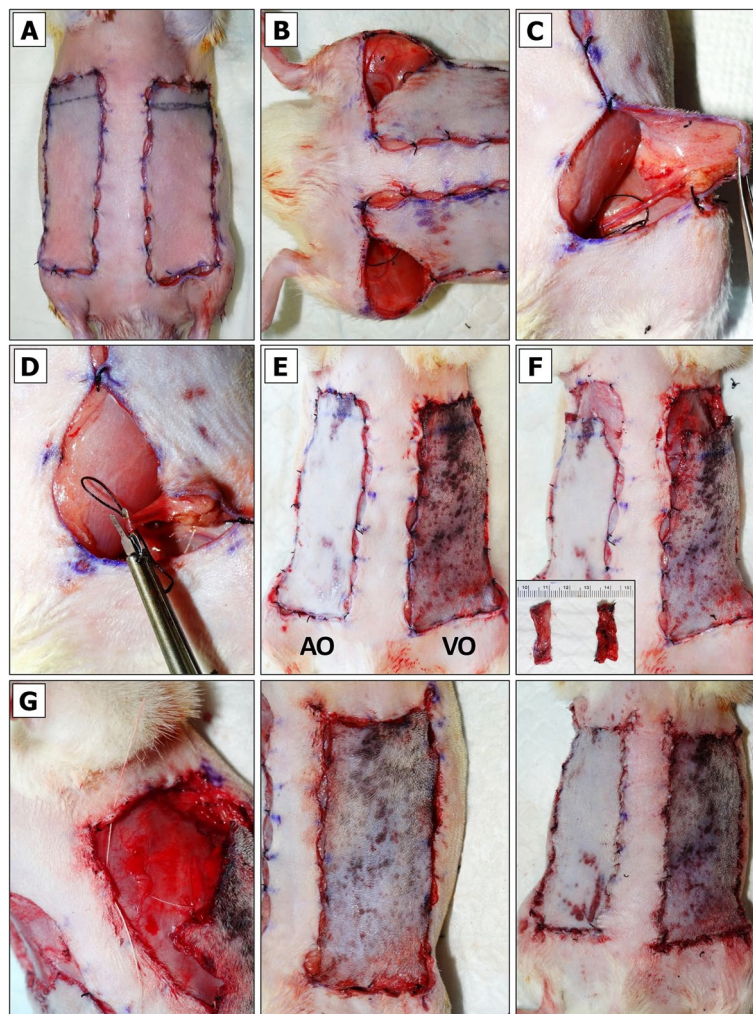


Fig. 9 Induction of secondary ischemia (SI). **A** BEFAF appearance after REP₁. **B** Flap preparation for selective vessel clamping. **C** Inspection of blood flow restoration in the pedicle prior SI. **D** SIEV clamping. **E** BEFAF appearance after selective SIEA (AO) or SIEV (VO) vessel occlusion. **F** B_{AO} and B_{VO} biopsy excision. **G** Final flap closure

flap are connected to a narrowed tissue using an absorbable suture. Here one may use the corner stitch mattress suturing technique [79]. Next, the center and remaining intermediate points (Fig. 9G, middle panel) are connected together. The same is done for the opposite side.

3. At this point, PVA sponge implantation may take place. One PVA piece is inserted using Adson forceps underneath the P, M and D portions of each flap. Control sponges may be inserted in the outer area of a flap. Alternatively, a small pocket may be opened on the animal's back.
4. A DPBS-moistened gauze is placed over the right flap. The left flap is positioned into place using a running suture technique with non-absorbable permanent suture (suggested directions of suturing are presented in Additional File 2, Fig. S8).
5. The flaps and surrounding areas are wiped with moistened gauze to remove the traces of blood and betadine solution.
6. The animal is flipped into a prone position. 10 mL of saline is injected sc to supplement bodily fluids lost in the animal during this extensive surgical procedure.
7. Isoflurane flow is decreased to 0% so that the animal receives only 100% Oxygen.
8. The gross appearance of the flaps is recorded by digital photography (Fig. 9G, right panel).

9. Once the animal begins to awaken, we typically put a protective Elizabethan collar prior to returning the animal to a new padded cage with fresh food and water (Additional File 2, Fig. S9). The collar should be applied loosely so that it rotates around the neck.
10. The HDPE tubes with collected tissue specimen are placed in -80°C freezer for storage.
11. All waste is removed, sharps disposed in specified containers, and all surgical instruments are washed, cleaned, and autoclaved at this point.

Post-surgical Animal Monitoring

When in distress, rodents can self-mutilate or cannibalize the ventral flap. If spotted on time, dehiscence may be fixed by suturing, but in the case of large opening the animal should be euthanized. When in doubt, the attending veterinarian should always be consulted. To prevent self-destructing behavior, Elizabethan collars should be used instead of restraining jackets that cause immobility and thus will compromise flap healing. Although male rats adapt to these collars quicker than female rats, a careful pre-operative introduction of the collars to all animals is strongly advised. Despite the pre-operative preconditioning with the collar, female rats will often refuse to eat/drink after the surgery but will quickly pick up on any exposed sutures once the collar is removed. Some leaner rats may access the bottom of the flap even in the presence of the collar (Additional File 2, Fig. S9). To avoid animal self-mutilation issues, many researchers choose to create the dorsal flaps as in the classical 1965 McFarlane experiment [80–84]. However, one should note that dorsal flaps represent RPFs and thus a different flap healing model compared to the APFs.

Surgery-related stress can be reduced by introducing an animal to a habitat with novel enrichment devices and dietary treats. While animal socialization is otherwise certainly encouraged, the post-operative animals (and in general retired breeder males) should be housed separately so that the collars may be used safely, and animal food/water intake would be tracked more accurately. Food pellets, dough diet and/or nutritional special needs recovery diet gels (commercially available from Bio-Serv (Flemington, NJ) or other vendors) should be placed on the floor postoperatively for easy access. Rodent diet may also be medicated. Post-surgical animal well-being should be constantly monitored at least twice per day. Animal weight should be recorded every other day. Post-surgical pain relief is available if it does not interfere with the aims of the study as some pain-relieving therapeutic compounds are known to impede or accelerate an inflammatory response and change the gene/protein expression

patterns. The suggested example of POAMS is provided as Additional File 1.

Non-survival Surgery

Preparation for Procedure

1. The HDPE tubes are labeled for appropriate specimen. A suggested label may contain a unique animal number, code for treatment, indication of left or right flap side (R/L), day of harvest and an abbreviated name of a harvested segment, e.g., “174,871, A, L7D”).
2. 10% buffered formalin container and histology cassettes are labeled for appropriate specimen.
3. A rubber bucket is filled with ice pellets. If PVA sponges were implanted, then 2.0 mL Eppendorf tubes are filled with PVA sponge lysis or other buffer, depending on the type of subsequent wound exudate (WE) analysis, and placed on ice. Flat-tip tweezers are prepared to handle the sponges.
4. Dewar flask is prefilled with LN₂ for immediate tissue freezing. We suggest using curved HDPE tube grabbing scissors.
5. CO₂ levels are checked in the euthanasia cart. Isoflurane and oxygen tank levels are checked in the anesthesia cart.

Flap Harvest

1. The animal is placed in the anesthetic sedation chamber prefilled with 4–5% isoflurane gas and kept there for up to 4 min.
2. 4% (larger rats) or 3% (smaller rats) isoflurane flow is redirected into the nose cone.
3. Once the animal is placed onto an underpad, which covers a heating pad, the digital photos of the flap appearance are taken. The functional outcome (full survival, partial failure, or total loss) of flaps exposed to SI should be evident by day 5, whereas flap fate following other treatments may be evaluated at later end-points. Figure 10A illustrates experimental situations, when the evaluation of flap survival percentage (FS%) by digital planimetry is not necessary (Fig. 10A, left panel – left flap, middle panel – both flaps) and when it is required (Fig. 10A, right panel – both flaps).
4. If the flaps are going to be divided into the proximal (P), medial (M) and distal (D) segments, a measuring ruler is placed on the top of a flap. Each flap is marked with either one dot, dotted or a solid line that would separate it into three equal portions. NOTE: this step should be performed on a

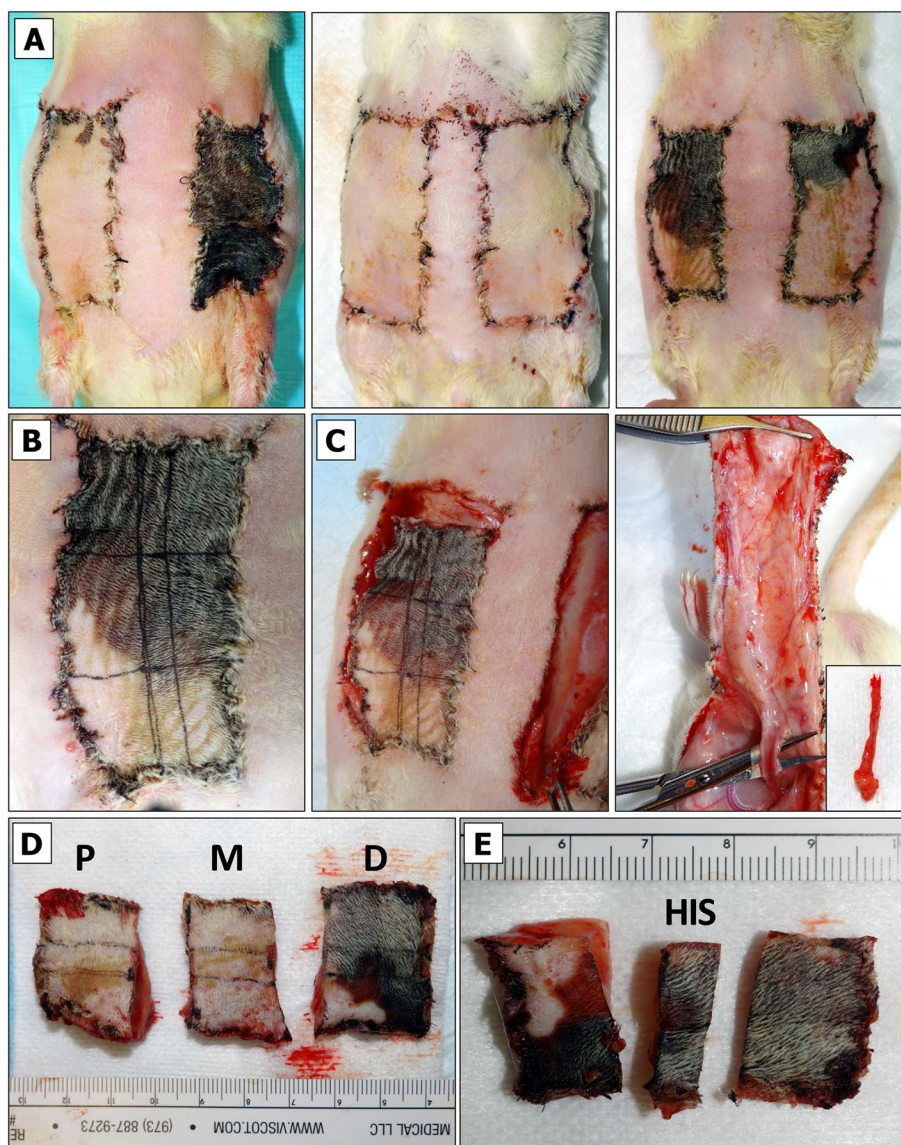


Fig. 10 Flap tissue harvest. **A** Flap appearance and different surgical outcomes (full survival, partial or complete failure) at chosen end-point. **B** Flap division into thirds and longitudinal sections. **C** Removal of sutures and flap excision. **D** Inspection of pedicle function. **D** Physical flap division into the proximal (P), middle (M) and distal (D) portions. **E** Isolation of longitudinal section out of D portion of excised flap for the subsequent fixation and histological (HIS) or immunohistochemical (IHC) analysis

living animal when the flaps are in fully extended position. If needed, the animal paws may be taped. If the IHC specimen is to be taken out of each portion, then two horizontal lines are drawn along the entire flap as shown in Fig. 10B.

5. All running sutures are disrupted and removed. One-by-one, the flaps are dissected along the wound margins and Mayo scissors are used to lift one flap after another from the wound bed. The status of the pedicle is inspected and POAMS form (Additional File 1) is used to indicate if it is

functional or compromised. A fully functional vessel will be visibly dilated and pumping the blood (Fig. 10C). Obstructed vessel will have a dark blood clot or will be clear of the blood.

6. At this point, all PVA sponges may be retrieved if any were implanted previously. These sponges should be cleaned from the tissue prior to placing them into the pre-labeled Eppendorf tubes stored on ice. WE is collected though repeated compression of each sponge with flap-tip tweezers, and the samples are diluted if necessary.

7. If the flap is going to be divided into the P, M and D regions as shown in Fig. 10D, it should preferably be cut into the thirds while it is still attached to the pedicle. Alternatively, the entire flap may be cut at the base, transferred onto a sterile Petri dish kept on ice and divided over there. Optionally, the pedicle can be excised out of the P region for a separate histological evaluation of other types of analysis. Whichever technique the surgeon chooses, he/she should stay consistent and adhere to the chosen sequence of flap harvest procedure throughout the entire course of experiment.
8. For IHC, the middle longitudinal strip is cut out of each flap's segment (Fig. 10E). A specimen is placed into a dedicated IHC cassette skin facing up. Edema will be the most prominent in the P segment of the flap, making it the thickest segment out of three. CRITICAL: the tissue strip should be laid straight and should not be twisted. The cassette is submerged in 10% formalin and incubated at RT for at least 48 h.
9. The remaining flap segment is placed in a pre-labeled HDPE tube, which is then submerged in LN₂. Even though the tissue may be small compared to the volume of the tube, it will less likely stick to the walls of the tube and will be easier to retrieve after freezing.
10. Other flap segments are processed in the same manner as described above.
11. For major vital organ harvest 5% (or greater) isoflurane flow is used to overdose the animal and then excise all organs of interest after its exsanguination. If organ harvesting is not required, then the gauze is placed over both excisional wounds and the animal is moved into the clean cage for euthanasia. The CO₂ flow rate is adjusted at 5 L/min and exposure to CO₂ is continued for at least five minutes after respiratory arrest. Euthanasia may be confirmed by cervical dislocation (for rats < 200 g in weight) or bilateral thoracotomy. NOTE: other methods of euthanasia may be used as per approved IACUC study protocol.
12. Animal carcass is placed in a biohazardous waste bag, which is disposed of according to Institutional LAS rules. Typically, this entails attaching a label with a specific information, logging animal death, leaving a carcass in a dedicated freezer or cold room, and concluding a unique animal cage tag.
13. The surgeon's working area is cleaned and sanitized. All surgical tools are washed, placed in the autoclave pouches/bags or trays, and then sterilized in the autoclave.

Results

The quantitative and qualitative analytical techniques of the collected biological specimens include but are not limited to planimetric flap survival analysis, histology (HIS) [85], immunohistochemistry (IHC), laser capture microdissection [86], flow cytometry (FC) [87], proteomic, metabolomic or transcriptomic analyses [88, 89]. These specimens may also be used to derive secondary analytes, such as EVs, which are typically analyzed for their biophysical properties (quantity, size, charge, optical redox ratio) and/or internal cargo consisting of proteins, lipids and nucleic acids [90–92].

The principles of planimetric analysis are described in Additional File 2, Fig. S10 and Fig. S11. Total and either necrotic or viable areas in the digital photos can be determined with the aid of a “Measurement Log”, “Quick Selection” and “Ruler” tools available in Adobe Photoshop or ImageJ software. The percentage of flap viability (FV%) or flap survival (FS%) is calculated as the necrotic flap area minus the total flap area divided by the total flap area (in square millimeters) multiplied by 100.

We also provide several simulated statistical flap survival data analysis examples in GraphPad Prism 9.5.0 software (Additional File 3 and Additional File 2, Fig. S12). The differences between the matched left and right flap survival may be estimated by the paired Student's T-test (Additional File 3, Example 1, and Additional File 2, Fig. S12, upper left panel). The before and after treatment effects (e.g., baseline versus PI versus REP₁ vs SI) within each flap of different animals may be evaluated by one-way repeated measures (RM) ANOVA (Additional File 3, Example 2, and Additional File 2, Fig. S12, upper right panel). For example, if the normalized phosphorylated Akt (p-Akt) protein expression effects were compared between the male and female animal groups consisting of 5 rats per each, we would be using two-way RM-ANOVA (Additional File 3, Example 3, and Additional File 2, Fig. S12, bottom left panel). A good source of explanation when and how to use fully-nested ANOVA without interaction is provided by John H. McDonald in his topic “Nested Anova” [93], which implies that if we would have 7 randomly selected rats, with 2 flaps created within each under different ischemic conditions, and if we would carry out 4 independent skin oxygenation measurements (one before the flap raising surgery in the spots of future-to-be flaps and then on POD 2, POD 5 and POD 9) with three repetitive measurements per each region of the flap each time, then our model could be analyzed either by “pure” Model II random-effects model-based nested ANOVA or by model I mixed-effects model-based nested ANOVA. In yet another example, if 14 male and 14 female non-littermate rats were randomly selected and assigned into 2 groups with 7 rats of

each gender per each, and these groups would receive an external treatment (e.g. tobacco vapors vs control water vapors) prior to BEFAF surgery, where one flap would be subjected to 4 h of PI alone and contralateral flap to 4 h PI, and then to 2 h of SI (e.g., AVO) after 12 h of REP₁, the nested ANOVA model would treat male and female rats as sub-groups and their flaps—as sub-sub-groups nested within these sub-groups. Furthermore, the distinct P, M and D segments of these flaps, if measured individually, would be treated as sub-sub-sub-groups. But if an overall flap viability % was measured at a single time point, e.g., POD 9, we could apply three-way 2×2×2 RM-ANOVA (Additional File 3, Example 4, and Additional File 2, Fig. S12, bottom right panel). In the provided example, values stacked in sub-columns would represent a set of matched or repeated measures values (4 h PI vs 4 h SI). Means of cells that differ only by one factor would be compared using post-hoc Šidák test, reporting the multiplicity-adjusted p-values for each comparison at alpha=0.05 (95% CI). Residual, homoscedasticity and quantile–quantile (QQ) plots would also be provided. An excellent feature of this type of analysis using GraphPad is the option to calculate cell/row/column means and grand means, which aid in plotting different results while considering or ignoring subject's gender (see Additional File 3).

The tissue sections are quite large and there will be room to place only two replicate sections on each slide for HIS analysis. We prefer MT stain over H&E, as it readily reveals new and old collagen structures, extent of inflammatory infiltration, edema, and newly formed vessels. Depending on the degree of necrosis, the left and right sides of tissue section may appear heterogenous. If there is no possibility to digitize the slides using an automated or semi-automated hardware/software, then manual image collection via conventional or polarized light microscopy may be performed in a following manner: (a) the image of the entire flap segment is taken at the lowest (4x) magnification and medium to low sharpness; (b) the upper, middle, and lower sections of the P, M or D flap regions are taken at higher magnification (10× or 20×) making sure these sections slightly overlap; (c) The images are then combined together using Adobe Photoshop or any other graphic design software to produce one seamless high-quality image (Figs. 11 and 12).

We stress the importance of presenting high resolution histological stain images of the flaps that are indispensable for diagnostic result interpretation in the full-thickness wound healing studies. Several images of the same area should be taken to reduce the risk of getting blurry poor-quality images (Additional File 2, Fig. S13). In our experience, the thickness of GT may be estimated from the 10× magnification micrographs (Fig. 13, left upper panel), while 20× and higher magnification

micrographs are suitable for quantitative vessel analysis (Fig. 13, left bottom panel). While vascular density and angiogenic budding may be visualized in sectioned flap tissues stained with H&E (Fig. 13, left bottom panel) or MT dyes alone (Fig. 13, right upper panel), staining with specific endothelial phenotype markers such as PECAM-1, vWf and/or CD34 (Fig. 13, right bottom panel) may be preferred. Vascular inflammation that causes endothelial barrier disruption and tissue edema can also be studied using BEFAFs. Some proteins that are involved in endothelial barrier recovery, e.g. Hsp27 [94], are expressed in rat flaps (data not shown). 20× and higher magnification micrographs are suitable for the gross tissue cellularity analysis (Fig. 14, left panel), including the presence of mature adipocytes and tissue infiltration with nucleated hematopoietic cells, namely neutrophils and macrophages (identifiable by their characteristic polymorphic and euchromatic nuclei, respectively, and by their positive staining reaction with CD45) (Fig. 14, right panel). Collagen deposition and collagen fiber alignment can be examined at 10× magnification following MT or Sirius-Red staining (which can distinguish between different collagen types). Currently there are several automated free and open-source ImageJ and more sophisticated MATLAB software plugins created to analyze different types of scientific HIS/IHC images.

Additional File 2, Fig. S14 confirms that proteins implicated in flap tissue healing and regeneration processes (e.g., MMP-9, VEGF, Angiogenin etc.) can be isolated directly from the collected WE or from the fluid extracted from the implanted PVA sponges. The isoleucine and hydroxyproline quantity in acid hydrolysates of each PVA implant will reflect total protein and collagen content. Specific cell populations can be isolated by FC from the WE filtered through a 70 μm cell strainer. For instance, a purified (>95%) population of wound macrophages as determined by F4/80 staining can be yielded by magnetic cell sorting using mouse anti-CD11b tagged microbeads [95]. A mixture of WE with specific lysis buffer to determine the latent and active matrix metalloproteinase profile by gelatin zymography [96] and various growth factor/cytokine/chemokine levels by ELISA [97] or IB may provide critical information on the healing trajectory of a wound and its suitability for advanced biological therapies [98–101].

Finally, one may choose to isolate proteins, mRNA or EVs from different flap segments using the materials and isolation procedures as suggested in Additional File 2. These biological cues may be analyzed in individual animals, but to minimize technical assay-to-assay variations, it is generally acceptable to summarize the individual animal responses following biological sample pooling.

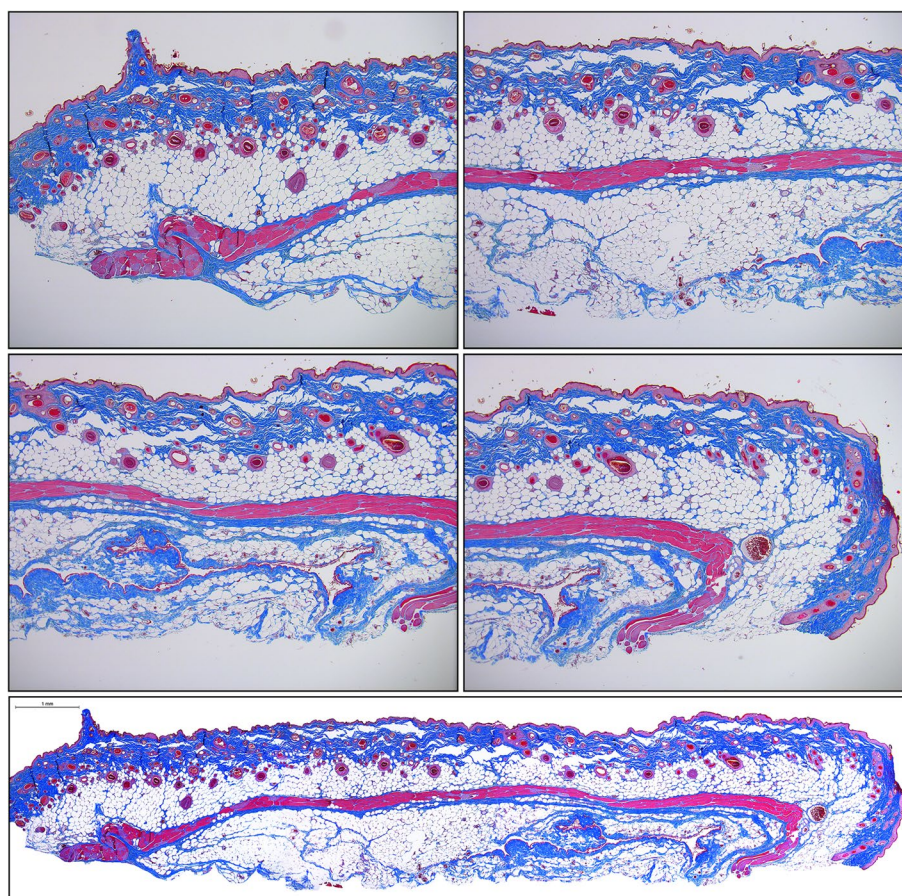


Fig. 11 Individual unprocessed 4× magnification micrographs of histological Masson's Trichrome-stained sections of male rat's middle left-side BEFAF segment before (upper panel) and after (bottom panel) manual image stitching procedure to generate one seamless image. This flap with an estimated 100% viability was harvested 48 h post-reconstructive surgery, where the left-side flap was exposed to 4 h PI, 2 h REP₁ and 4 h of SI (AVO), whereas right-side flap was exposed to 4 h PI, 6 h REP₁ and 4 h of SI (AVO). The digital stitching procedure started with opening all three raw unprocessed images in Adobe Photoshop and extending the canvas of the first image to the right side. Then a second image was dragged as a layer onto the first image trying to align and eliminate overlapping features. Lastly, the third and fourth images were placed underneath. The exposure of each layer was adjusted to match the previous layer using "Levels" properties. The darker edges were eliminated by using "Dodge" tool. Finally, the layers were merged and cropped to eliminate blank spaces on the top and bottom sides. The background of the final image was cleaned from debris by selecting the background with the "Quick Selection" tool, deleting it, and replacing it with the white color. The final image was then adjusted for contrast and sharpness. Scale bar = 1 mm

Figure 15 demonstrates the bilateral flap model's advantage over a traditional unilateral flap model in an experimental design where the superiority, equivalence, or non-inferiority effects of the desired preventative/prophylactic treatment is being evaluated. In this practical example of BEFAF model validation, the experimental treatment was based on activated platelet-rich plasma (aPRP), whereas a control treatment consisted of equal volume of activated platelet-poor plasma (aPPP). PRP is plasma enriched with a platelet concentration above that typically contained in whole blood. The platelets are best known for their importance in clotting blood. At the same time, alpha granules in platelets contain numerous growth factors (GFs) [102]. Besides their

well-established roles in growth, migration, chemotaxis, division and differentiation processes, GFs can protect distinct types of body cells against ischemic or oxidative damage in vitro [103–107]. Consequently, different fields of medicine have increasingly experimented with aPRP substances containing 5–10 times greater amounts of GFs [108–110]. Upon release from calcium, thrombin and/or type I collagen-activated platelets [110], those cues have been shown to speed up the healing process of excisional full-thickness wounds [111–113]. aPRP administration has been shown to improve the survival of naïve pedicled RPFs or APFs in different experimental animal models in vivo [114–116]. Similarly, human patients with and without diabetes receiving aPRP

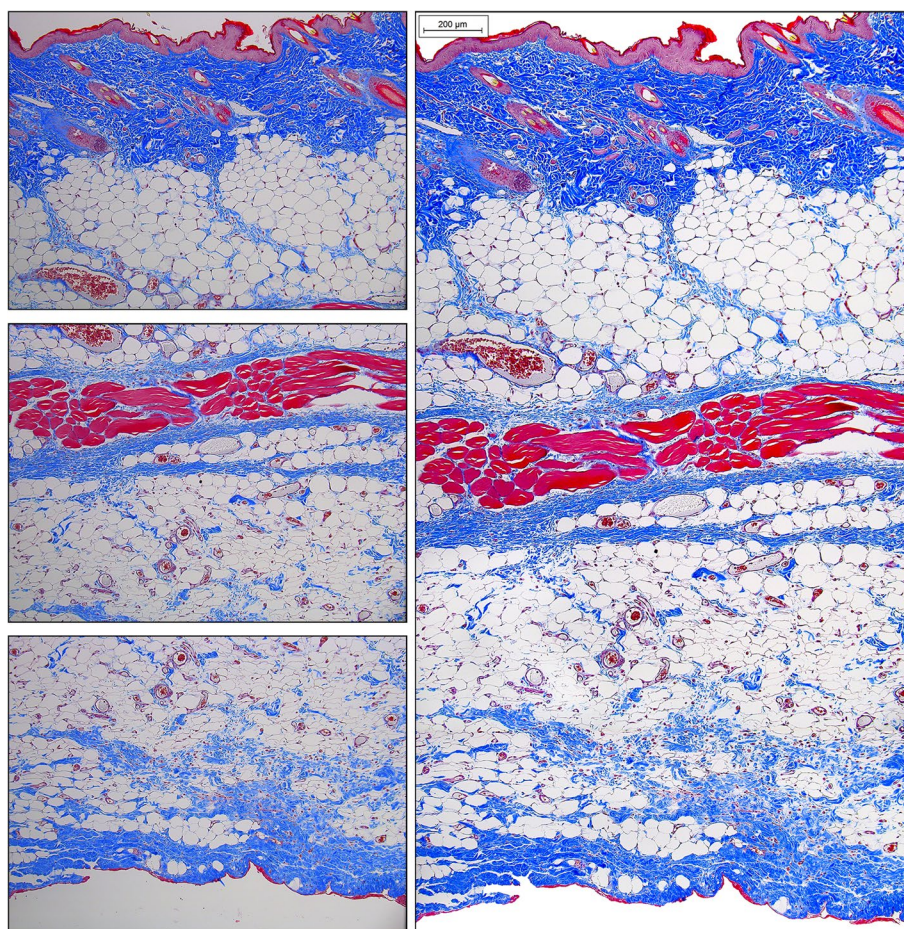


Fig. 12 Individual unprocessed 10× magnification micrographs of histological Masson's Trichrome-stained top, center, and bottom layer of male rat's distal left-side BEFAF segment before (left panel) and after (right panel) manual image stitching procedure to generate one seamless image. The digital stitching process starts with opening all three raw unprocessed images in Adobe Photoshop and extending the canvas of the first image down. Then a second image was dragged as a layer onto the first image trying to align and eliminate overlapping features (indicated by yellow arrows). Lastly, the third image was placed underneath. The exposure of each layer was adjusted to match the previous layer using "Image > Adjustments > Levels" tool by sliding the input levels to the left or to the right. The darker edges of each image (if any) were eliminated by applying "Dodge" tool. Finally, the layers were merged and cropped to eliminate blank spaces on the left and/or right sides. The final seamless image was adjusted for contrast, exposure, and sharpness. Scale bar = 200 μm

injections or patch treatments saw a significant reduction in their wound areas [117, 118].

In a traditional experimental design, e.g., using a unilateral rotational APF as shown in Fig. 15A, a total of 14 animals (7 animals/group) would be theoretically required to evaluate the significance of experimental treatment effect on ischemic flap survival. But in the BEFAF model, where a distal portion of the right flap was treated with aPRP, while the left side was treated with control aPPP substances, animal number needs were reduced by half (Fig. 15B). The efficacy of PI, SI and reperfusion between the flaps could be visually documented to disclose any peri-operative variations of tissue response to physical manipulation (Fig. 15B, upper left panel). In the provided

example, the efficacy of PI and the rate of primary reperfusion that was visually assessed after 2 h post-PI showed no noticeable difference between the left-side and the right-side BEFAFs (Fig. 15B, upper left panel, left and middle images). After 6 h both flaps were entirely perfused, and ready to be subjected to the SI insult (AVO). This is important, because in the event of significant dissimilarity or spontaneous thrombosis following the PI, the treatment outcome becomes arguably invalid. At the end of the study, marking a designated wound healing stage (e.g. at POD 8), FV% was evaluated by the planimetric analysis (Fig. 15B, upper left panel, right image). To standardize the detection of molecular and cellular tissue responses, the flaps were harvested and divided

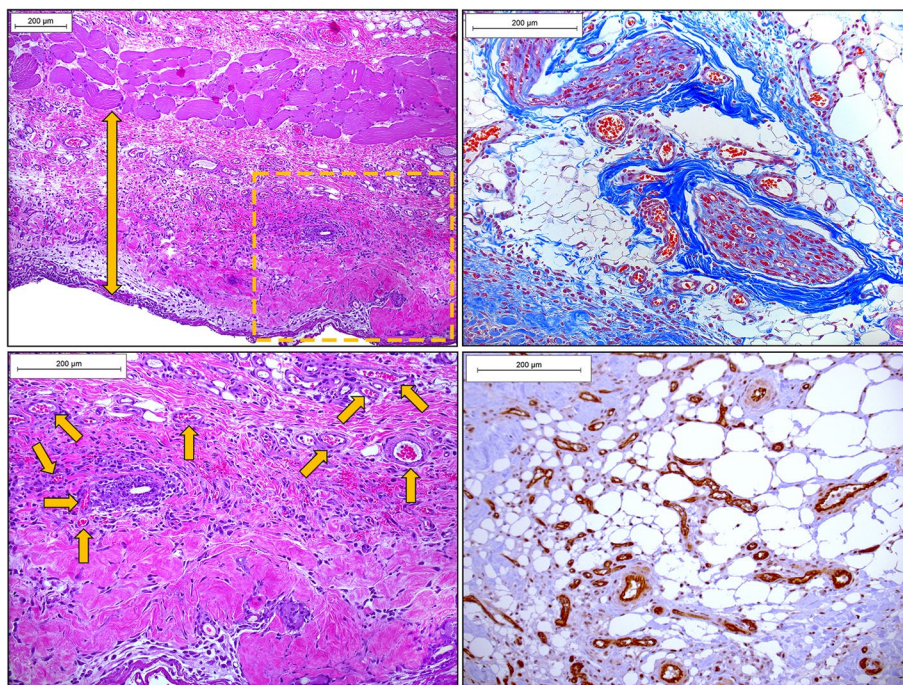


Fig. 13 Left panel. Representative 10× (upper panel) and 20× (bottom panel) magnification micrographs of the bottom layer of Hematoxylin and Eosin (H&E)-stained histological section of male rat's middle right-side BEFAF segment 7 days post-surgery, where both flaps were subjected to 4 h PI, 2 h REP1 and 4 h of SI, namely, VO (left flap) or AO (right flap). The deep fascia layer underneath *Panniculus carnosus* contains the granulation tissue (GT). GT thickness (indicated by yellow arrows) and vascularity (best visible in the 20× zoom image of yellow rectangular region) will vary depending on the flap harvest time and the severity of the ischemic insult. Scale bar = 200 µm. Right upper panel. Representative 20× magnification micrograph of the bottom layer of Masson's Trichrome (MT)-stained histological section of proximal right-side BEFAF segment next to the pedicle 5 days post-surgery where both flaps were subjected to 4 h of PI, 2 h (right flap) or 6 h (left flap) REP₁ and 4 h of SI (AVO). Both flaps survived 100% and had functional pedicles. At this magnification, the perfused blood vessels could be examined and counted manually. Bigger collagen-enclosed formations are regions of sprouting angiogenesis and neovasculogenesis. MT stain: blue color = collagen connective tissue fibers; dark red color = muscle and keratin; bright red color = red blood cells (erythrocytes); dark purple/black = cell nuclei; purple = cytoplasm; white = adipose (fat) cells. Bottom panel. The representative 20× magnification micrograph of PECAM-1 (CD31) positive-vessels. 10% formalin-fixed 4 micron cut paraffin sections of the embedded distal segment of male SD rat flap 7 days after the BEFAF surgery, where the flaps were exposed to either 2 h or 6 h of PI, were stained with recombinant rabbit polyclonal anti-CD31 antibody (RM1006) (Abcam, #ab281583) at 1/400 dilution after heat-mediated antigen retrieval with Tris/EDTA buffer pH 9.0. Brown color reaction was detected with chromogen diaminobenzidine (DAB). Scale bar = 200 µm

into three parts to separate D, M and P regions. Each region was then cut into three equal weight segments – the left segment is used for protein extraction, the right segment – for mRNA or EV isolation and the middle segment – for HIS (Fig. 15B, bottom right panel). In this experimental design, the control tissue could be obtained from the ventral unwounded centerline, and the dilated pedicle could be carefully dissected from P region for HIS evaluation.

As shown in the right panel of Fig. 15B, a vast array of rat species-reactive and compatible antibodies is available to assess tissue survival, inflammation, proliferation and even remodeling status by semi-quantitative Western Blotting technique. When assessing basal/constitutive or inducible signaling activation status of kinases, phosphatases, and especially transcription factors in injured tissues, it is a good practice not only to examine

the extent of protein phosphorylation on their activating residues, but also to quantify the total (phosphorylated and non-phosphorylated) level of proteins, because their stability and expression dynamics may depend on wound healing stage as well as functional interactions with other proteins. For example, while the peak activation of signal transducer and activator of transcription protein-3 (STAT3) due to an inflammatory reaction and ischemia mostly occurs at the first stage of wound healing [119, 120], it is also prominent in later stages of wound repair, such as angiogenesis and re-epithelization as it can be re-activated by the vascular epidermal growth factor (VEGF) receptors [121, 122]. For example, from analysis of Fig. 15B, it can be suggested that despite sustained inflammatory cytokine levels (e.g., IL-6) which theoretically should activate JAK2/STAT3 pathway [123], the decreased phosphorylation of STAT3 on activating

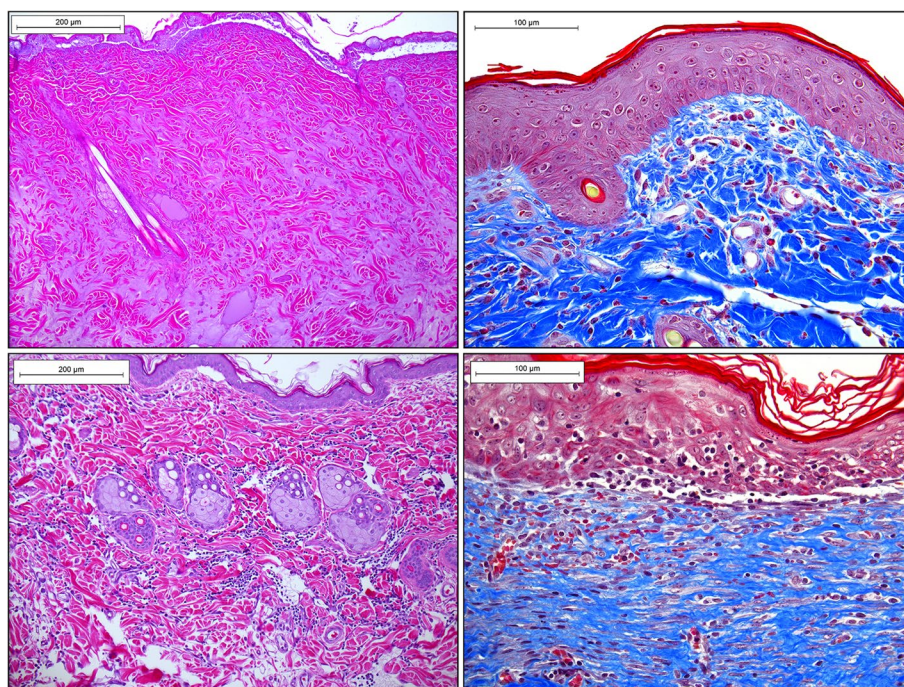


Fig. 14 Left panel. Representative 20× magnification microscopy images of top layer of Hematoxylin and Eosin (H&E)-stained histological sections of distal (upper panel) or proximal (bottom panel) left-side BEFAF segments 5 days post-surgery where both flaps were subjected to 4 h of PI, 2 h (right flap) or 6 h (left flap) REP₁ and 4 h of SI (AVO). The D segment of left-flap failed which was confirmed by the dominance of acellular devitalized regions. The P segment of left-flap appeared healthy but showed a marked infiltration of inflammatory cells above the *Panniculus carnosus* layer. H&E stain: blue/dark purple – nuclei; pink – cytoplasm; magenta – collagen. Scale bar = 200 μm. Right panel. Representative 40× magnification microscopy images of top layer of Masson's Trichrome (MT)-stained histological section of middle right-side BEFAF segment 5 days post-surgery where both flaps were subjected to 4 h PI, 2 h REP₁ and 4 h of SI, namely, AO (right flap, upper panel) or VO (left flap, bottom panel). At this magnification, the researcher can evaluate the integrity and health status of epidermis, as well as inflammatory cell infiltration into the upper layers of the skin. Scale bar = 100 μm

Tyr705 residues in the D flap region that failed to heal following severe ischemic insult and control treatment could be mainly attributed to the STAT3 protein degradation. This depletion likely occurred due to high protease activity and as a result of keratinocyte, fibroblast, and vascular endothelial cell death, as manifested by the augmented Caspase-3 Asp175 phosphorylation and severely delayed type I collagen fiber deposition at this later stage of wound healing, compared to the non-necrotic P region of the same flap containing high activated pro-survival Akt kinase levels that function upstream of proteolytic caspases. Caution must also be taken to interpret the fold-differences of protein expression results based on traditional house-keeping protein normalization. Some of those proteins might not be as stable as expected during the wound healing and deep tissue regeneration process. In our experience, the expression of growth factor receptor bound protein 2 [Grb2; UniProt database Accession No: P62994] and to a lesser degree, beta-Actin (UniProt: P60711) were relatively stable over the excisional large ventral wound healing process, whereas the glyceraldehyde-3-phosphate dehydrogenase (GAPDH;

UniProt: P04797) and alpha-tubulin (UniProt: P68370) levels fluctuated a lot and were not suitable for protein normalization.

In a similar fashion, BEFAFs may be utilized to evaluate the biological effects of a preconditioning surgical delay technique, which triggers the expression and activation of angiogenic genes [124] and potentially stimulates cell-to-cell communication through EVs. In this procedure, the left or right flap is raised, placed back onto the resultant wound, and left to fully heal for 7 – 14 days. Thereafter BEFAF surgery is performed on both sides of the animal creating a desired type of flap. These flaps are allowed to heal under physiologically normal or perturbed conditions. Pre-surgical and post-surgical responses of interest (e.g., the rate and degree of tissue reoxygenation) as well as tissue survival are then compared between the control (acutely raised) and paired experimentally preconditioned (delayed) flap tissue at designated POD(s) (Fig. 16). The expected EV size distribution derived from 2 g of naive abdominal flap is shown in Additional File 2, Fig. S15, proving that the isolation, separation, and detection of relatively polydisperse crude small and large EV

sub-population fractions from collagenase-digested fasciocutaneous rat tissues is feasible.

Discussion

Undoubtedly, both small and large animal models play a vital role in biomedical and veterinary sciences research. The significance, as well as limitations, of small animal models have been discussed in multiple reviews, now spanning decades [125–129]. While some concerns and debates have been raised regarding poor pre-clinical animal model translation into human clinical trials or routine medical practice [130, 131] potentially due to the lack of evaluation of methodology in the surgical animal studies [129, 132, 133], the scientific and didactical value of such models cannot be denied. Animal models have historically been used for basic and applied research, testing the tolerance and efficacy of pre-clinical treatments, implants and medical devices, and toxicity screening during pharmaceutical drug or vaccine development [43, 134]. They are essential for exploring cell survival and death mechanisms, as well as learning/training specific techniques and acquiring tissue handling, suture ligation, anastomosis skills, and more [135–137].

Surgical animal models have been instrumental in understanding the intricacies of diabetic ulcer and burn wound healing, cartilage repair, multifactorial musculoskeletal and cardiovascular disorders, vascular grafting choice, influence of co-morbidities and IRI on superficial or excisional wound closure, deep tissue repair and regeneration capacity. These models contribute significantly to the fields of transplant, plastic, and reconstructive surgery, extending beyond learning basic anatomy or microsurgery techniques [135, 138–140].

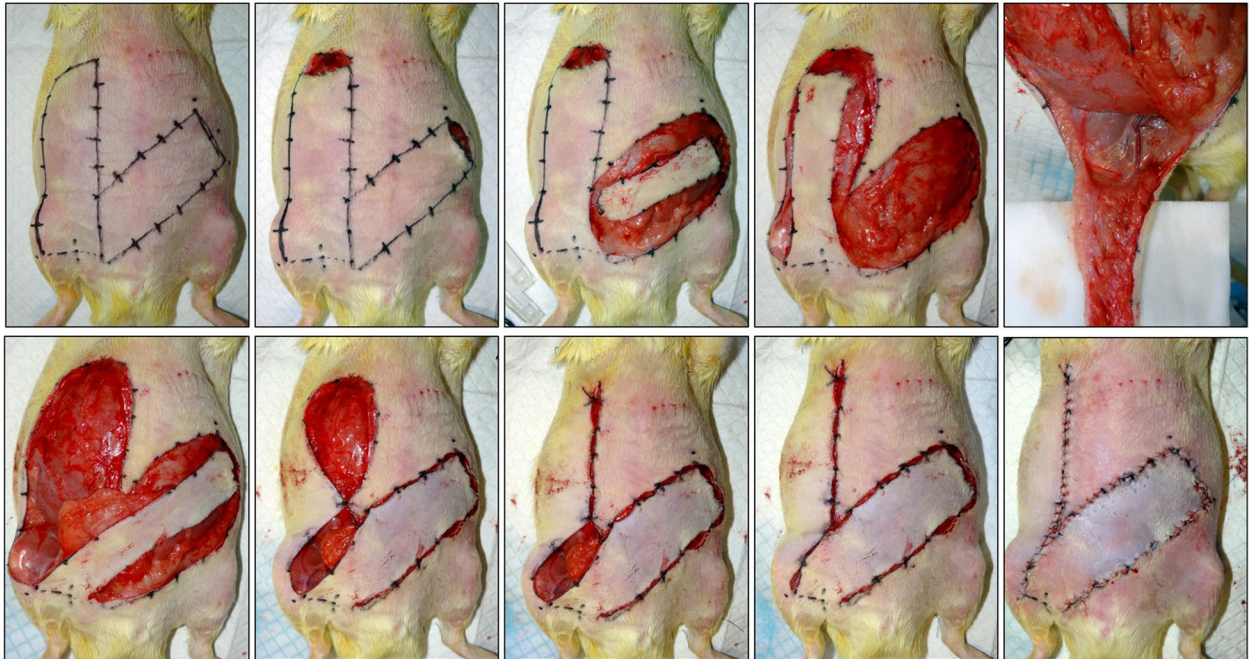
The standardized and continuously updated protocols detailing the scope and duration of procedures aid as effective teaching tools. They help in establishing and maintaining a reproducible animal model suitable to answer fundamental basic and translational research questions, gaining competence in pre-operative/post-operative animal care, post-operative complication handling techniques, and learning to apply the three R's (Reduction, Refinement, Replacement) principles [134].

However, tissue flap models that aim to teach specific surgical skills and simultaneously study reparative processes still lack firm guidelines and standardization [141, 142]. The presented reconstructive surgery model using

(See figure on next page.)

Fig. 15 Application of conventional unilateral versus BEFAF model to explore the effects of prophylactic/therapeutic surgical flap treatment on tissue susceptibility to secondary ischemia. Experimental design: the SIEV and SIEA of the pedicle are clamped with a single atraumatic non-serrated S&T 11 mm vascular clamp for 2 h to induce primary ischemia (PI). After 2 h the clamp is released, and the flap is allowed to reperfuse for 6 h (R1) prior to repeated SIEV and SIEA clamping to induce a secondary ischemia (SI) by arteriovenous occlusion (AVO) lasting for 4 h. Once the SI is alleviated, the secondary reperfusion (R2) begins until the endpoint (POD 8). Experimental and control treatments are introduced prior to R1 and R2 events by intradermal injection into the distal flap region. **A** In a traditionally used ischemic flap model, a single fasciocutaneous flap is created and rotated around a pivotal axis point (the base of the pedicle may remain intact or may be severed to minimize a residual microvascular inflow) per animal. Power analysis suggests that if the flap survival percentage response within each subject after SI is normally distributed with standard deviation of 10, and assuming the attrition rate is 10%, then if the true difference in the experimental and control means is 20 as to be calculated by independent two-tailed Student's T-test, we would need to study 7 experimental and 7 control subjects (total $N = 14$ animals) to be able to reject the null hypothesis that the population means of two groups are equal with probability (power) of 0.9. The Type I error probability associated with this test of this null hypothesis is 0.05. **B** Left panel. To perform the similarly powered experiment with twice as few animals per group, two 3×9 cm BEFAF flaps were created within each animal: one flap was assigned to the treatment, and the opposite flap – to the control group. Experimental treatment solutions were prepared from blood collected through cardiac puncture of previously sacrificed inbred Lewis strain rats ($N = 12$). Mixed arteriovenous blood was collected in 4.5 mL BD Vacutainer® Sodium Citrate (0.105 M, 3.2%) glass tubes that were centrifuged at $400 \times g$ for 10 min at 4°C to separate plasma from red blood cells. Plasma with a buffy coat layer was collected into sterile 5 mL Eppendorf tube and spun at $1,000 \times g$ for 10 min to sediment platelets and leukocytes. Half of supernatant was collected into 2 mL Eppendorf tube (*platelet poor plasma, PPP*). The remaining supernatant was gently mixed with the pellet and transferred into a separate 2 mL Eppendorf tube (*platelet rich plasma, PRP*). PPP and PRP solutions were activated by adding 1 M CaCl_2 to the final concentration of 22.2 mM and incubating the tubes in a dry bath at 37°C for 1 h. Growth factors (GFs) were released from the precipitated platelets into the liquid fraction after final centrifugation step at $10,000 \times g$ for 10 min. Supernatants were passed through sterile $0.22 \mu\text{m}$ pore size syringe filter, combined into a single aPPP or aPRP stock solution and stored at -20°C until further use. Pooling was intended to eliminate or minimize the heterogeneity of aPRP or aPPP content so that all flaps would receive an equal concentration of GF-enriched or control filtrate. 250 μL of aPRP was injected to the distal portion of inner right-side flap (R), while the 250 μL of aPPP (control) was injected in the similar location of the left-side flap (L) prior to the start of R1 and R2 events. At POD 8, the paired flaps were photographed, harvested, and divided into equal proximal (P), medial (M) and distal (D) regions that in turn were subdivided into left, central, and right segments. Right panel. The left segment of P, M or D regions was flash frozen, crushed into powder, lysed, pooled from seven 10-month old retired breeder Lewis strain male rats (mean weight = 542 g), and used for protein separation by lithium dodecyl-sulfate polyacrylamide gel electrophoresis (LDS-PAGE) at 130 V constant in 4–12% gradient NuPAGE gels followed by protein transfer onto $0.22 \mu\text{m}$ nitrocellulose membranes at 30 V constant for 90 min, and protein expression analysis by immunoblotting (IB) using the primary antibodies against indicated total or phosphorylated (p-) forms of antigens of interest and horseradish peroxidase-conjugated secondary antibodies. Chemiluminescent proteins bands were visualized by a Kodak Image Station 440CF equipped with the Carestream image analysis software (Kodak, New York, NY) following 5 min strip incubation with 20 ml SuperSignal™ West Dura Extended Duration Substrate (TFS, # 34076)

A. 14 ANIMALS (7 treated and 7 control)



B. 7 ANIMALS with 7 paired BEFAFs for 4 h PI, 6 h R1, 4 h SI (AVO), R2

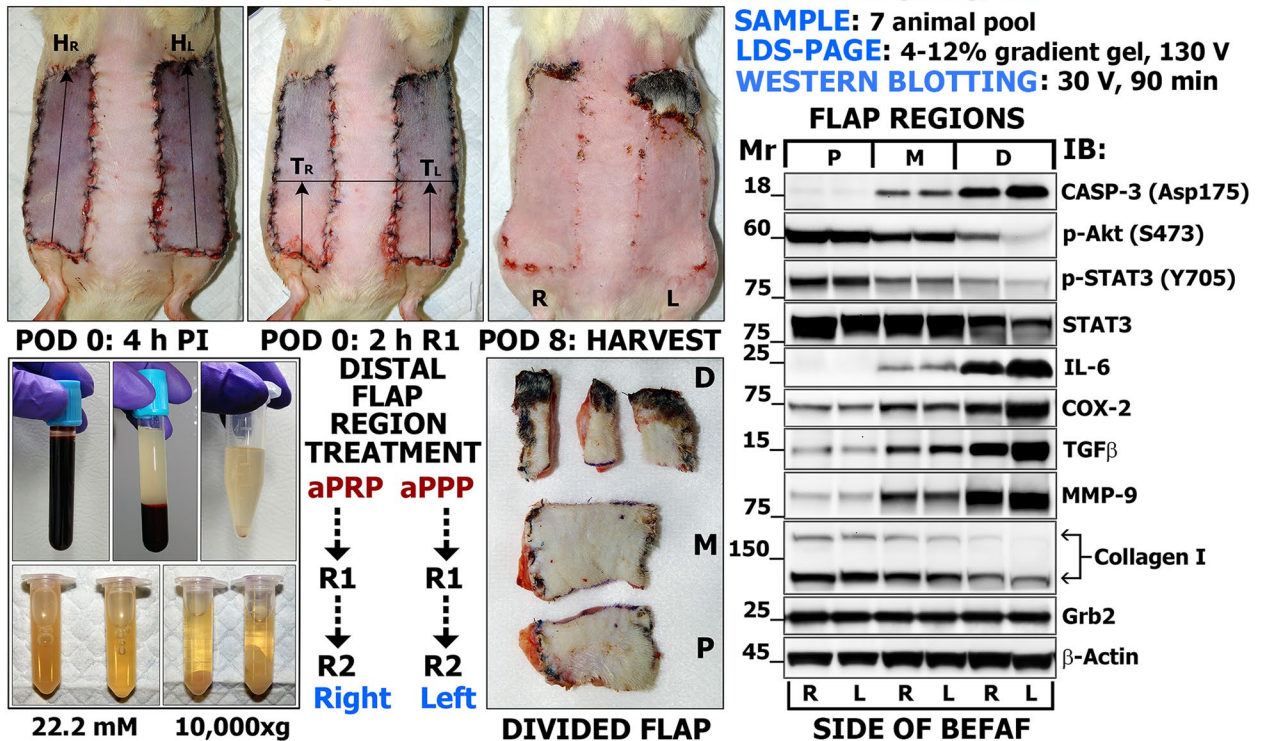


Fig. 15 (See legend on previous page.)

BEFAFs shows promise as a more effective, less time consuming and cheaper alternative for standardized validation of therapeutic targets, diagnostic and prognostic

biomarkers as well as clinical treatment strategies than conventional unilateral wound healing animal models. This model is based on compound APFs and can

be readily modified to represent either pedicled or free flap under varied clinical situations. One may assess the impact of endogenous or exogenous factors such as sex/gender, age, diet, physical activity, metabolic and chronic diseases on quantitative measures such as the rate of flap reoxygenation, vascularization, cell metabolism, migration, signaling and overall tissue survival. The BEFAF model is ideally suited to explore the molecular profiles associated with ischemic susceptibility or tolerance and to evaluate biomarkers for early prediction of flap outcome. Moreover, the procedure can be scaled and reproduced using other animal species (e.g., mice, rabbits, minipigs).

The concept of a model featuring symmetrical, three-sided, caudally based bilateral skin flaps in rats was first described by Ozcan et al. [143]. Their model created the RPFs resulting in a predictable and persistent necrosis. Elegantly, these RPFs have been used to assess the efficacy of preventative therapy (superoxide dismutase). Similarly, the tolerance of bilateral RPFs to the absence of vascular flow through the main feeding vessel and to the genetically modified autologous fibroblast therapy was investigated by Machens et al. [144]. Because these previous studies utilized RPF model, the flaps did not undergo a transient PI event – a prerequisite if one must mimic the autologous tissue transfer and IRI. In addition, the previously described models were not adapted to take intermittent biopsies for longitudinal or repeated measures data analysis and did not simulate temporary flap failure and salvage procedure.

As demonstrated by Figs. 15 and 16, BEFAFs, which effectively simulate the microvascular free flaps subject to spontaneous vascular complications, can be used to reveal effective therapies for prevention of flap loss or improvement of flap survival after re-exploration and

salvage. Aside from an evaluation of flap healing rate, the animals may successfully undergo non-invasive *in vivo* microscopy. For instance, differences in left- and right-side flap vascularization and reoxygenation rates may be examined by combined photoacoustic and Doppler ultrasound imaging, while dynamic metabolic changes in tissues may be assessed by intravital microscopy [84, 145]. Temporal levels of intradermal nitrogen or oxygen may be measured by using specific needle-type microsensors or implants [146].

Finally, the BEFAF model can be adapted to evaluate a relative contribution of the recipient wound bed to APF survival. In such a case, a sterile silicone sheet is placed between the flap and the abdominal muscle. The sheet is sutured to the edges of a flap to prevent its movement, which may cause a physical damage to the pedicle [147]. Although some wound bed isolation studies conducted on single animals showed a significant reduction of flap survival rates [148, 149], other investigators did not see a significant difference in functional flap outcome, but agreed that induction of potent pro-inflammatory response by a foreign material might conceal the true driving forces of the healing process [150]. Ultimately, if superficial wound healing—not flap survival—is a preferable measure of outcome, then unipedicle or bipedicle ventral bilateral flaps can be created to establish a gradual ischemic environment followed by punching a series of excisional wounds. These wounds may be further reinforced using silicone splinters to overcome the excisional wound healing by contraction [151]. A similar bilateral flap approach may be applied to the dorsal RPFs that are described in the classical 4 × 10 cm McFarlane's model [80, 152]. Theoretically, even APFs may be rotated along their axis to end up on the dorsal side and vice versa: the caudally based RPFs may be transposed

(See figure on next page.)

Fig. 16 Application of BEFAF model to explore the effects of pre-conditioning surgical flap delay technique. A representative workflow of flap delay technique using pedicled flaps in 10-month-old male SD rat is shown. **A** Left flap was raised, placed back onto the resultant wound, and left to fully heal for 7 days. **B** Delayed flap healing status on 7th POD. **C** BEFAF surgery was performed on the left and right sides of the animal creating regular non-advanced flaps. During this type of surgery, the microvascular supply at the base of the flap (pedicle) is left intact. **D** Flaps were allowed to heal under normal conditions for 2 days. **E–F** On 2nd POD for the right flap and on the 9th POD for the delayed left flap, biopsies were taken from the distal portion of each flap for molecular analysis. **G** The flaps were advanced and allowed to heal for 7 more days. **H** Flap healing efficacy was evaluated on 9th POD for the control (C) flap and POD 16th POD for the delayed (D) flap. **I** Flaps were harvested for additional comparative and correlative analysis with flap reoxygenation that was evaluated by the combined photoacoustic (PA) and Doppler ultrasound (US) imaging (**J**). Ultrasound coupling gel was applied to the animal skin before the images were captured on selected regions (left panel) at the 12 mm focal depth using the Vevo2100 LAZR imaging system (VisualSonics Inc, Toronto, Canada), which operates LZ-250 transducer (21 MHz) frequency transducer and has 20 Hz tunable near-infrared light laser (680–970 nm). Besides B-Mode, which displays a greyscale two dimensional cross-section of tissue, 2-D images were acquired using 'Oxy-Hemo' mode, which collects data at 750 and 850 nm wavelengths, and then creates and displays a parametric distribution map of oxygenated Hemoglobin (oxyHb) and total hemoglobin (tHb) at a rate of 1 Hz (right panel). The imaging probe was positioned between the medial and distal segments on 1) the day of flap delay surgery on the R flap to take baseline flap oxygen saturation level measurement designated as R0; 2) on 2nd POD after left-side flap delay on the D flap to take acute reoxygenation response measurement designated as D2; 3) on 2nd POD after right-side flap raising surgery on the R flap to take acute reoxygenation response measurement (R2) and on the same day on the D flap to assess a secondary reoxygenation response designated as D9

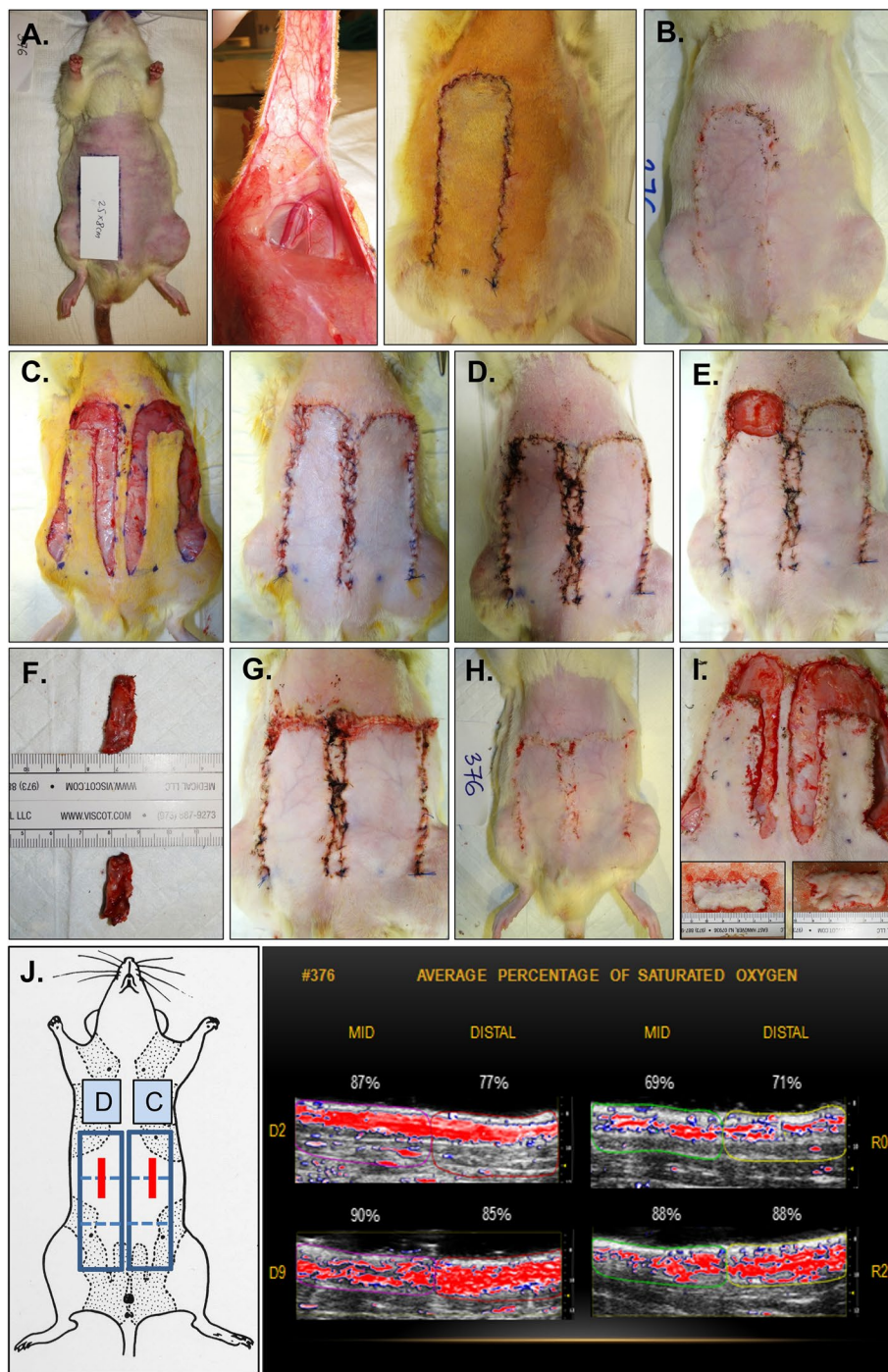


Fig. 16 (See legend on previous page.)

towards a ventral side, but we did not test whether such transposition flap model is feasible, and it remains unclear if rodent skin would be flexible enough to cover two simultaneously created excisional wounds.

While the results of standardized studies using BEFAFs may be appropriate to guide recommendations for

refining perioperative and post-operative flap management in specific human patient populations undergoing extensive reconstructive surgeries, this model presents challenges and has some limitations. The first or foremost challenge is vascular dissection. Using microsurgical techniques, SIEA and SIEV vessels can be divided,

and anastomosis can be performed under a microscope to directly simulate free flap surgery. As shown by other reports, this technique is feasible in rats that have smaller caliber vessels ranging from 0.3 mm to 0.8 mm in diameter, but it requires using a microvascular surgery microscope or high magnification loupes [153–158]. To simplify this highly specialized procedure and make it more readily accessible to non-medical novice and less experienced researchers, anastomosis can be simulated by using atraumatic vascular clamps, as described in this protocol. Undoubtedly, the physical separation of epigastric vessels using a suture thread presents a risk of damaging the vessel with a needle. In our hands, the non-medical researcher who had used magnifying loupes to perform a physical vessel separation procedure by passing a suture and a needle between the SIEA and SIEV, experienced 20% attrition per 20 raised flaps.

Next, in BEFAF model, the survival/failure rate and efficacy of re-integration of right flap in response to the desired treatment regimen can be compared to that of saline-treated left flap control or vice versa. However, based on the results of our experiments using the methylene blue dye injection into the distal flap areas, the diffusion may impact the opposite side if the amount of injected solution exceeds 500 μ L (in rats). It is also expected that the survival percent of left and right untreated flaps may slightly vary. Although this naturally occurring within-subject variation typically does not exceed 10% of total flap area, an excessive manipulation of flap pedicles or flap corners can introduce unwanted heterogenous effects. Moreover, a degree of hypoxia induced in the distal portions of the flaps may differ not only between two different strains of animals but also between the same-strain animals that are received from different vendors. For instance, we noticed that Lewis strain rats have relatively thin blood with less time needed for reperfusion, thus their flaps had a better chance of survival than the same type flaps created in SD strain rats. In turn, SD strain rats obtained from Charles River Laboratories were more susceptible to flap failure after the SI compared to SD rats received from Envigo. Thus, for purely procedural repeatability studies, all surgeries should be preferably performed using littermate animals obtained from the same vendor. Sex-, age- and diet-based differences should be considered as well: our preliminary data suggest that middle aged male rat flaps are more susceptible to IRI than female flaps, that young less obese rats heal quicker than elderly counterparts, and that while liquid versus solid chow diet does not have a significant impact on advancement flap survival per se, there are some changes in differential gene expression following the PI (manuscripts in preparation). Therefore, looking at combined versus isolated effects between fixed

or random factors during the multifactorial statistical flap survival and molecular tissue response data analysis is recommended. Moreover, we noticed that not all rats produce similar amount of WE during the flap healing process, but the underlying causes of this phenomenon needs to be investigated in future studies.

Finally, in some experimental settings, rodents are exposed to repetitive anesthesia, which may induce respiratory failure and overdose-related death, especially in light weight animals. Susceptibility to overdose may also depend on animal gender: in our hands, female rats were less prone to overdosing than male rats. If the animal stops breathing during anesthesia, cardiopulmonary resuscitation is possible. Repetitive checking of animal vital signs, timely decrease, or cessation of anesthesia and sufficient time gaps between serial animal sedation events decreases fatal outcomes.

Conclusions

Accurate comparisons between standardized complex wound healing studies would add to the translational knowledge base of complex tissue healing under normal and pathological conditions. BEFAFs may be used to investigate the spatiotemporal cellular and molecular responses to complex tissue injury and interventions simulating clinically relevant flap complications (e.g., secondary arterial, venous, or mixed ischemia) and therapeutic or surgical treatments (e.g., flap delay) in the presence or absence of confounding risk factors (e.g., substance abuse, irradiation, diabetes) or favorable wound-healing promoting activities (e.g., exercise). This technically challenging but feasible reconstructive surgery model eliminates inter-subject variability, while concomitantly minimizing the number of animals needed to achieve adequate statistical power. Overall flap experiments designed for studying the effects of SI may be lengthy, require good time management skills, visual aids, awareness, and stamina. They may appear too laborious for novice trainees but have the merit of simulating real-life clinical surgeries sometimes lasting more than 8 h. The described protocol of ischemic BEFAF model may serve as an aid for teaching basic vascular microsurgery techniques that focus on technical and non-technical skill acquisition in both medical and non-medical trainees.

Abbreviations

AO	Arterial occlusion
APF	Axial pattern flap
AVO	Arteriovenous occlusion
BEFAF	Bilateral epigastric fasciocutaneous advancement flap
D	Distal
DPBS	Dulbecco's Phosphate-Buffered Saline
EVs	Extracellular vesicles

FC	Flow cytometry
FV	Flap viability
FS	Flap survival
GF	Growth factor
GT	Granulation tissue
HDPE	High-density polyethylene
H&E	Hematoxylin and eosin (stain)
HIS	Histology
IB	Immunoblotting
IHC	Immunohistochemistry
LN ₂	Liquid nitrogen
M	Middle/medial
MT	Masson's Trichrome (stain)
NC	Nucleic acid
P	Proximal
PBS	Phosphate-Buffered Saline
PI	Primary ischemia
POAMS	Post-operative animal monitoring sheet
POD	Postoperative day
PPE	Personal protective equipment
PVA	Polyvinyl alcohol
REP ₁	Primary reperfusion
REP ₂	Secondary reperfusion
RPF	Random pattern flap
SC	Subcutaneous
SD	Sprague–Dawley (rat strain)
SI	Secondary ischemia
SIEA	Superficial inferior epigastric artery
SIEV	Superficial inferior epigastric vein
siRNA	Small interfering ribonucleic acid
VO	Venous occlusion
WE	Wound exudate

Supplementary Information

The online version contains supplementary material available at <https://doi.org/10.1186/s12575-023-00227-w>.

Additional file 1. Animal perioperative and post-operative record.

Additional file 2: Figure S1. Surgical tools used in flap raising surgery. **Figure S2.** A variation of BEFAF model using a quadruplicate biopsy design, biopsy excision and the temporary protection of wound bed after a partial excision of the tissue. **Figure S3.** Examples of vessel ligation, split SIEA isolation and reinforced pedicle clamping using two clamps (D). **Figure S4.** Principles of simple-interrupted suturing. **Figure S5.** Temporary sutures placement order and directions for the left-side BEFAF with real-time suturing order examples. **Figure S6.** Visual directions on how to pass a needle through the corners of left and right base of the BEFAF. **Figure S7.** Example of flap failure due to the development of spontaneous venous thrombosis. **Figure S8.** Principles of simple continuous running suturing at the end of the survival surgery. **Figure S9.** Animal recovering after major survival surgery. **Figure S10.** Preparation for digital planimetric analysis using commercial "Adobe Photoshop" software. **Figure S11.** Digital planimetric analysis using commercial "Adobe Photoshop" software. **Figure S12.** Examples of statistical simulated flap-study related data analysis. **Figure S13.** Non-acceptable and acceptable quality of raw unprocessed micrographs of Masson's Trichrome-stained histological sections of rat's BEFAF. **Figure S14.** Protein expression in rat's BEFAF wound exudate or PVA sponge fluid. **Figure S15.** Expected size distribution and concentration of extracellular vesicle (EV) subpopulations isolated from unperturbed abdominal rat skin.

Additional file 3. Examples of statistical flap data analysis and visualization.

Acknowledgements

The authors are grateful for excellent technical support, guidance and animal care received from TJU Department of Laboratory Animal Services staff, and especially thank Veterinary Technician Evelyn Skoumbourdis, MS, RLATG

as well as animal caretaker Victoria Jackson. The authors thank Dr. John R. Eisenbrey and sonographer Maria Stanczak, MS, RDMS, RVT for their services providing animal PA-DUS imaging, and TJU's Translational Research/Pathology Core facility manager Dr. Zhijiu Zhong and his staff for their excellent histological stain services.

Authors' Contributions

EP: Conceptualization, Methodology, Project Administration, Resources, Funding acquisition, Writing - Reviewing and Editing. RH: Methodology, Project Administration, Supervision, Writing - Reviewing and Editing. JH: Supervision, Resources, Writing - Reviewing and Editing. EA: Investigation, Visualization, Formal analysis, Writing - Original draft preparation. All authors reviewed the original and revised manuscript.

Authors' Information

EA is a long-term member of Wound Healing Society (WHS), American Society for Biochemistry and Molecular Biology (ASBMB) and American Society for Investigative Pathology (ASIP). She completed her undergraduate and postgraduate studies in the Faculty of Natural Sciences at Vytautas Magnus University (VDU) (Kaunas, Lithuania), and received the B.S. in Biology (2001), M.S. in Molecular Biology & Biotechnology (2003) and PhD in Biochemistry (2007) degrees from VDU's Department of Biology. She joined Prof. Boris N. Kholodenko's Systems Biology and Cell Signalling Networks research group at the Department of Pathology, Anatomy and Cell Biology at Thomas Jefferson University (TJU) (Philadelphia, PA, USA) as a Research Assistant in 2004 to study the receptor tyrosine kinases (RTK)-mediated cell signalling. While at TJU, she completed her postdoctoral research in Cancer Signal Transduction as a NIH NIAAA T32 grant-funded trainee. In 2014, EA joined the Department of Otolaryngology – Head and Neck Surgery (TJU) to serve as a Research Instructor. She continued her research investigating cellular pathway interactions in reparative wound healing, and mentored Department's residents teaching them basic biochemical analysis methods and surgical animal model techniques. Currently, EA holds a Research Scientist position at the Beckman Institute for Advanced Science and Technology, which is a unit of University of Illinois Urbana-Champaign (Urbana, IL, USA) dedicated to interdisciplinary research. She coordinates human clinical research studies in Prof. Stephen A Boppart's Biophotonics Imaging Laboratory that collaborates with pharmaceutical industry companies and takes part in projects focused on human skin conditions, ear diseases and cancer. She has recently joined the International Society for Extracellular Vesicles (ISEV) to study extracellular vesicles and their signalling roles in normal tissues and cancer. Dr. Aksamitiene's interests also include method validation and procedure optimization strategies to achieve repeatable and reproducible studies.

EDP is a Professor at Department of Otolaryngology – Head and Neck Surgery at Thomas Jefferson University (TJU) (Philadelphia, PA, USA), an Executive Vice President at Jefferson Health and the President of the Jefferson Medical Group. He graduated from Perelman School of Medicine at the University of Pennsylvania in 1986 and completed his residency in Hospital of University of Pennsylvania (HUP). He received a fellowship from Stanford University Hospital (Stanford, CA) and is Board-Certified in Otolaryngology as well as Facial Plastic and Reconstructive Surgery. EDP holds active ENT physician appointments at Thomas Jefferson University Hospital (TJU) and Methodist Hospital Division of TJUH (Philadelphia, PA). He is interested in selectivity and response characteristics of human olfactory neurons which would help identifying treatment for taste and smell disorders. He also specializes in thyroid carcinoma and thyroid, parathyroid and rhinoplasty surgery. EDP has been a consecutive P-50 NIH Grant Co-Investigator, served on the Sidney Kimmel Medical College Dean's Diversity, Equity & Inclusion (DEI) Council (Philadelphia, PA) and led the Educational and Research Foundation for the American Academy of Facial Plastic and Reconstructive Surgery (AAFPRS) Domestic Violence Project. EDP serves on the Board of Trustees of Wilmington University (New Castle, DE, USA). He and Patrizio Cernetti co-founded medical devices company, which has patented a drug delivery device that attaches to any smart phone. He wrote the first BoTox dose response paper and originated the Sonic Rhinoplasty technique. As a leader and mentor adept at building strong cross-functional teams, EDP continuously supports medical student scientific research rotation programs teaching how to translate various pre-clinical surgical animal models to human clinical research.

JBH is a Professor and Vice-Chair for Research at Department of Pathology, Anatomy and Cell Biology at Thomas Jefferson University (TJU) (Philadelphia, PA, USA). JBH trained in biochemistry with Drs. J.M. Tager and E.C. Slater at the University of Amsterdam, focusing on mitochondrial metabolism. He received his Ph.D. degree in 1972. During this time, he also worked with Dr. H.A. Krebs in Oxford, UK, on the integration of mitochondrial and tissue redox metabolism. He then pursued postdoctoral studies with Dr. Lars Ernster in Stockholm, Sweden, after which he joined the faculty of the University of Nairobi in Kenya. Dr. Hoek was introduced to alcohol research in 1981, when he joined the group of Dr. Emanuel Rubin at Hahnemann University in Philadelphia. The alcohol research group moved in 1986 to TJU. JBH has held numerous leadership and advisory positions in the alcohol research field. He has served on several NIH and NIAAA study sections, and from 2004 to 2008 was a member of the NIAAA National Advisory Council. He is currently a member of the Medical Advisory Council of the Alcoholic Beverages Medical Research Foundation (ABMRF). JBH is Associate Editor for Reviews and Commentaries for Alcoholism, Clinical and Experimental Research. He also chairs the Publication Committee of the Research Society on Alcoholism. JBH is engaged in multiple scientific collaborations in the U.S. and internationally. He serves on the steering committee of the German Liver Systems Biology consortium "HepatoSys," and he works closely with the newly established Systems Biology Center at University College Dublin, Ireland. NIAAA has honoured JBH with the Mark Keller Award. The research in interdisciplinary JBH's laboratory focuses on the unique regenerative capabilities of the liver and how they are distinctively regulated by mitochondrial calcium signalling and alcohol metabolism. JBH's laboratory developed different rodent alcohol consumption models to analyse the integrated signalling responses in liver and other tissues and study the adaptive or maladaptive modification of these responses by acute and chronic ethanol exposure. Some of his models were adapted to investigate the impact of alcohol on ischemic wound healing. RNH is a Professor at Department of Otolaryngology – Head and Neck Surgery at Thomas Jefferson University (TJU) (Philadelphia, PA, USA). He received his undergraduate degree from Yale University (New Haven, CT, USA), and began his medical education at Jefferson Medical College (Philadelphia, PA) where he received his MD degree. He was elected to the Alpha Omega Alpha Medical Honour Society and was awarded the S. MacCuen Smith Memorial Prize in Otolaryngology. RNH completed his internship in General Surgery followed by a surgical residency and specialization in Otolaryngology – Head and Neck Surgery at TJU Hospital (Philadelphia, PA). RNH was then chosen for a highly specialized Fellowship in Facial Plastic and Reconstructive Surgery, sponsored by the American Academy of Facial Plastic and Reconstructive Surgery (AAFPRS) at the University of California (Los Angeles, CA, USA). He returned to TJU in 2006 and became the Director of the Division of Facial Plastic and Reconstructive Surgery. He is highly active in teaching the latest advancements and techniques in plastic surgery to residents and fellows. RNH is Double Board-Certified Facial Plastic and Reconstructive Surgeon at TJU Hospital (Philadelphia, PA) and a fellow of the American Academy of Surgeons. As a facial plastic surgeon, RNH specializes solely in plastic surgery of the face, head, and neck, including facial nerve paralysis treatment, corrective surgery for facial defects, microsurgery, reconstruction of cancer patients and extensive post-traumatic deformities. RNH has been named a Castle Connolly Top Doctor and a Philly Top Doc yearly since 2017. He is one of five surgeons regularly serving the humanitarian Children's Rehabilitation Institute and Surgery Program (C.R.I.S.P.).

Funding

This research did not receive any specific grant from funding agencies in the public, commercial, or not-for-profit sectors, and was supported by the Department of Otolaryngology – Head & Neck Surgery, Thomas Jefferson University, Philadelphia, PA.

Availability of Data and Materials

Data sharing is not applicable to this article as no datasets were generated or analyzed during the current study.

Declarations

Ethics Approval

All animal experiments were conducted in accordance with ARRIVE guidelines as well as policies of the NIH Guide for the Care and Use of Laboratory Animals (NIH Publications No. 8023, revised 1978) and were approved by the Institutional Animal Care and Use Committee (IACUC) of Thomas Jefferson University (TJU) (IACUC protocols #01713, #01481, #020181).

Competing Interests

The authors declare no competing interests.

Author details

¹Department of Otolaryngology – Head and Neck Surgery, Thomas Jefferson University, 925 Chestnut St., 6Th floor, Philadelphia, PA 19107, USA. ²Present address: Beckman Institute for Advanced Science and Technology, University of Illinois Urbana-Champaign, 405 N. Mathews Ave | M/C 251, Room 4357, Urbana, IL 61801, USA. ³Department of Pathology, Anatomy and Cell Biology, Thomas Jefferson University, 1020 Locust St, Room 527, Philadelphia, PA 19107, USA. ⁴Sidney Kimmel Medical College, 31st Floor, 1101 Market Street, Philadelphia, PA 19107, USA.

Received: 13 June 2023 Accepted: 14 December 2023

Published online: 17 January 2024

References

- Baker SR. Reconstruction of Facial Defects. In: Flint PW, editor. Cummings Otolaryngology - Head & Neck Surgery. 1. 5th ed. Philadelphia: Elsevier; 2010. p. 342–63.
- Baker SR. Local flaps in facial reconstruction. Philadelphia: Saunders; 2014.
- Krishnan R, Garman M, Nunez-Gussman J, Orenge I. Advancement flaps: a basic theme with many variations. *Dermatol Surg.* 205;31:986-94.
- Heather S, Kriet JD, Clinton H. Advancement flaps. *Plast Aesthet Res.* 2022;9:25.
- Taylor GI, Palmer JH. The vascular territories (angiosomes) of the body: experimental study and clinical applications. *Br J Plast Surg.* 1987;40(2):113–41.
- Tsur H, Daniller A, Strauch B. Neovascularization of skin flaps: route and timing. *Plast Reconstr Surg.* 1980;66(1):85–90.
- Oswald P, Tilgner A, Schumann D. The influence of postoperative vessel occlusion on the viability of free microvascular skin-fat flaps and island flaps in rats. *J Reconstr Microsurg.* 1988;4(5):403–7.
- Szade A, Grochot-Przeczek A, Florczyk U, Jozkowicz A, Dulak J. Cellular and molecular mechanisms of inflammation-induced angiogenesis. *IUBMB Life.* 2015;67(3):145–59.
- Manosalva C, Quiroga J, Hidalgo AI, Alarcon P, Anseoleaga N, Hidalgo MA, et al. Role of lactate in inflammatory processes: friend or foe. *Front Immunol.* 2021;12:808799.
- Jog NR, Caricchio R. The role of necrotic cell death in the pathogenesis of immune mediated nephropathies. *Clin Immunol.* 2014;153(2):243–53.
- Perng C-K. Recent advances in postoperative free microvascular flap monitoring. *Formos J Surg.* 2013;46(5):145–8.
- Chen Y, Shen Z, Shao Z, Yu P, Wu J. Free flap monitoring using near-infrared spectroscopy: a systemic review. *Ann Plast Surg.* 2016;76(5):590–7.
- Geis S, Prantl L, Dolderer J, Lamby P, Mueller S, Jung EM. Postoperative monitoring of local and free flaps with contrast-enhanced ultrasound (CEUS)–analysis of 112 patients. *Ultraschall Med.* 2013;34(6):550–8.
- Wei FC, Demirkan F, Chen HC, Chuang DC, Chen SH, Lin CH, et al. The outcome of failed free flaps in head and neck and extremity reconstruction: what is next in the reconstructive ladder? *Plast Reconstr Surg.* 2001;108(5):1154–60. Discussion 61-2.
- Biglari B, Buchler A, Reitzel T, Swing T, Gerner HJ, Ferbert T, et al. A retrospective study on flap complications after pressure ulcer surgery in spinal cord-injured patients. *Spinal cord.* 2014;52(1):80–3.
- Kroll SS, Netscher DT. Complications of TRAM flap breast reconstruction in obese patients. *Plast Reconstr Surg.* 1989;84(6):886–92.
- Moran SL, Serletti JM. Outcome comparison between free and pedicled TRAM flap breast reconstruction in the obese patient. *Plast Reconstr Surg.* 2001;108(7):1954–60. Discussion 61-2.
- Kinsella JB, Rassekh CH, Wassmuth ZD, Hokanson JA, Calhoun KH. Smoking increases facial skin flap complications. *Ann Otol Rhinol Laryngol.* 1999;108(2):139–42.
- Fujioka M. Factors predicting total free flap loss after microsurgical reconstruction following the radical ablation of head and neck cancers. *ISRN Plast Surg.* 2013;2013(Article ID 952971):5.

20. Nahabedian MY, Momen B, Manson PN. Factors associated with anastomotic failure after microvascular reconstruction of the breast. *Plast Reconstr Surg.* 2004;114(1):74–82.
21. Wax MK, Rosenthal E. Etiology of late free flap failures occurring after hospital discharge. *Laryngoscope.* 2007;117(11):1961–3.
22. Iseli TA, Yelverton JC, Iseli CE, Carroll WR, Magnuson JS, Rosenthal EL. Functional outcomes following secondary free flap reconstruction of the head and neck. *Laryngoscope.* 2009;119(5):856–60.
23. Lie KH, Barker AS, Ashton MW. A classification system for partial and complete DIEP flap necrosis based on a review of 17,096 DIEP flaps in 693 articles including analysis of 152 total flap failures. *Plast Reconstr Surg.* 2013;132(6):1401–8.
24. Paddack AC, Frank RW, Spencer HJ, Key JM, Vural E. Outcomes of paramedian forehead and nasolabial interpolation flaps in nasal reconstruction. *Arch Otolaryngol Head Neck Surg.* 2012;138(4):367–71.
25. Baumeister S, Follmar KE, Zenn MR, Erdmann D, Levin LS. Strategy for reoperative free flaps after failure of a first flap. *Plast Reconstr Surg.* 2008;122(3):962–71.
26. Davison SP, Clemens MW, Kochuba AL. Anatomy of free flap failures: dissection of a series. *Mod Plast Surg.* 2013;3(3):89–95.
27. Novakovic D, Patel RS, Goldstein DP, Gullane PJ. Salvage of failed free flaps used in head and neck reconstruction. *Head Neck Oncol.* 2009;1:33.
28. Harreus U. Surgical errors and risks - the head and neck cancer patient. *GMS Curr Top Otorhinolaryngol Head Neck Surg.* 2013;12:Doc04.
29. Wong VW, Sorkin M, Glotzbach JP, Longaker MT, Gurtner GC. Surgical approaches to create murine models of human wound healing. *J Biomed Biotechnol.* 2011;2011:96918.
30. Luginbuhl A, Modest M, Yan K, Curry J, Heffelfinger R. Novel irradiated axial rotational flap model in the rodent. *JAMA Facial Plast Surg.* 2013;15(5):344–8.
31. Belmont MJ, Marabelle N, Mang TS, Hall R, Wax MK. Effect of photodynamic therapy on revascularization of fasciocutaneous flaps. *The Laryngoscope.* 2000;110(6):942–5.
32. Wax MK, Reh DD, Levack MM. Effect of celecoxib on fasciocutaneous flap survival and revascularization. *Arch Facial Plast Surg.* 2007;9(2):120–4.
33. Hart K, Baur D, Hodam J, Lesoon-Wood L, Parham M, Keith K, et al. Short- and long-term effects of sildenafil on skin flap survival in rats. *Laryngoscope.* 2006;116(4):522–8.
34. Taleb S, Moghaddas P, Rahimi Balaei M, Taleb S, Rahimpour S, Abbasi A, et al. Metformin improves skin flap survival through nitric oxide system. *J Surg Res.* 2014;192(2):686–91.
35. Vourtsis SA, Spyriounis PK, Agrogiannis GD, Ionac M, Papalois AE. VEGF application on rat skin flap survival. *J Invest Surg.* 2012;25(1):14–9.
36. McKnight CD, Winn SR, Gong X, Hansen JE, Wax MK. Revascularization of rat fasciocutaneous flap using CROSSEAL with VEGF protein or plasmid DNA expressing VEGF. *Otolaryngol Head Neck Surg.* 2008;139(2):245–9.
37. Polito F, Bitto A, Galeano M, Irrera N, Marini H, Calo M, et al. Polydeoxyribonucleotide restores blood flow in an experimental model of ischemic skin flaps. *J Vasc Surg.* 2012;55(2):479–88.
38. Yingxin G, Guoqian Y, Jiaquan L, Han X. Effects of natural and recombinant hirudin on VEGF expression and random skin flap survival in a venous congested rat model. *Int Surg.* 2013;98(1):82–7.
39. Mendes JJ, Leandro CI, Bonaparte DP, Pinto AL. A rat model of diabetic wound infection for the evaluation of topical antimicrobial therapies. *Comp Med.* 2012;62(1):37–48.
40. Roy S, Aksamitiene E, Hota S, Zhang LH, Sciarriano J, Baker AL, et al. Aging effects on pedicled fasciocutaneous flap survival in rats. *Head Neck.* 2016;38(Suppl 1):E1152–62.
41. Reyna RE, Feldmann ME, Evans ZP, Seung-Jun O, Chavin KD. Obesity alters rat abdominal flap survival. *Am Surg.* 2006;72(9):764–71. Discussion 71–2.
42. Karayel H, Kaya B, Caydere M, Terzioglu A, Aslan G. Prevention of unfavourable effects of cigarette smoke on flap viability using botulinum toxin in random pattern flaps: an experimental study. *Plast Surg (Oakv).* 2015;23(3):177–82.
43. Aksamitiene E, Baker AL, Roy S, Hota S, Zhang LH, Rodin J, et al. Biochemical effects of exercise on a fasciocutaneous flap in a rat model. *JAMA Facial Plast Surg.* 2017;19(4):303–10.
44. Kryger Z, Zhang F, Dogan T, Cheng C, Lineaweaver WC, Buncke HJ. The effects of VEGF on survival of a random flap in the rat: examination of various routes of administration. *Br J Plast Surg.* 2000;53(3):234–9.
45. Dolen UC, Sungur N, Koca G, Ertunc O, Bagci Bosi AT, Kocer U, et al. The vasodilator effect of a cream containing 10% menthol and 15% methyl salicylate on random-pattern skin flaps in rats. *Arch Plast Surg.* 2015;42(6):695–703.
46. Kuntscher MV, Hartmann B, Germann G. Remote ischemic preconditioning of flaps: a review. *Microsurgery.* 2005;25(4):346–52.
47. Shah AA, Arias JE, Thomson JG. The effect of ischemic preconditioning on secondary ischemia in myocutaneous flaps. *J Reconstr Microsurg.* 2009;25(9):527–31.
48. Farber N, Haik J, Weissman O, Israeli H, Winkler E, Zilinsky I. Delay techniques for local flaps in dermatologic surgery. *J Drugs Dermatol.* 2012;11(9):1108–10.
49. Scholz T, Evans GR. Impact of hypertonic and hyperoncotic saline solutions on ischemia-reperfusion injury in free flaps. *Plast Reconstr Surg.* 2008;122(1):85–94.
50. Zheng J, Xi S, Ding M, Li H, Xu W, Tang M, et al. Effects of venous super-drainage and arterial supercharging on dorsal perforator flap in a rat model. *PLoS One.* 2016;11(8):e0160942.
51. Camargo CP, Margarido NF, Guandelini E, Vieira GA, Jacomo AL, Gemperli R. Description of a new experimental model skin flap for studying skin viability in rats. *Acta Cir Bras.* 2014;29(3):166–70.
52. Godoy GR, Liebano RE, Correa JB, Hochman B, Ferreira LM. Capsaicin on the viability of random-pattern skin flaps in rats. *Acta Cir Bras.* 2010;25(5):440–3.
53. Prado RP, Liebano RE, Hochman B, Pinfildi CE, Ferreira LM. Experimental model for low level laser therapy on ischemic random skin flap in rats. *Acta Cir Bras.* 2006;21(4):258–62.
54. Gasteratos K, Paladino JR, Akelina Y, Mayer HF. Superiority of living animal models in microsurgical training: beyond technical expertise. *Eur J Plast Surg.* 2021;44(2):167–76.
55. Munhoz AM, Pellarin L, Montag E, Filassi JR, Tachibana A, Gebrim H, et al. Superficial inferior epigastric artery (SIEA) free flap using perforator vessels as a recipient site: clinical implications in autologous breast reconstruction. *Am J Surg.* 2011;202(5):612–7.
56. Wolfram D, Schoeller T, Hussl H, Wechselberger G. The superficial inferior epigastric artery (SIEA) flap: indications for breast reconstruction. *Ann Plast Surg.* 2006;57(6):593–6.
57. Pan H, Zheng Q, Yang S. Utility of proximally based sural fasciocutaneous flap for knee and proximal lower leg defects. *Wounds.* 2014;26(5):132–8.
58. Khandelwal S. An abdominal flap to save the right forearm and the hand, following a high-voltage electric burn in a child: a case report. *J Clin Diagn Res.* 2013;7(7):1473–5.
59. Aydin MA, Nasir S. Free SCIA/SIEA skin flap: a dual blood supply approach to groin region. *Microsurgery.* 2007;27(7):617–22.
60. Woodworth BA, Gillespie MB, Day T, Kline RM. Muscle-sparing abdominal free flaps in head and neck reconstruction. *Head Neck.* 2006;28(9):802–7.
61. Ou KL, Chen TM, Chen SG, Dai NT, Chang SC, Deng SC, et al. Three abdominal defects, three pedicled flaps. *Wounds.* 2013;25(11):305–9.
62. Choi JY, Chung KC. The combined use of a pedicled superficial inferior epigastric artery flap and a groin flap for reconstruction of a dorsal and volar hand blast injury. *Hand (N Y).* 2008;3(4):375–80.
63. Yavari M, Ghazisaidi MR, Hoseini Zahmatkesh S, Jahadi R. Comparison of sole to palm reconstruction using the combined medial plantar and medial pedis free flaps and abdominal pedicle flap for extensive palm injuries. *Acta medica Iranica.* 2010;48(4):214–7.
64. Chiu YH, Chang DH, Perng CK. Vascular complications and free flap salvage in head and neck reconstructive surgery: analysis of 150 cases of reexploration. *Ann Plast Surg.* 2017;78(3 Suppl 2):S83–8.
65. Chen KT, Mardini S, Chuang DC, Lin CH, Cheng MH, Lin YT, et al. Timing of presentation of the first signs of vascular compromise dictates the salvage outcome of free flap transfers. *Plast Reconstr Surg.* 2007;120(1):187–95.
66. Yu P, Chang DW, Miller MJ, Reece G, Robb GL. Analysis of 49 cases of flap compromise in 1310 free flaps for head and neck reconstruction. *Head Neck.* 2009;31(1):45–51.

67. Boissiere F, Gandolfi S, Riot S, Kerfant N, Jenzeri A, Hendriks S, et al. Flap venous congestion and salvage techniques: a systematic literature review. *Plast Reconstr Surg Global Open*. 2021;9(1):e3327.
68. Wu MY, Yang GT, Liao WT, Tsai AP, Cheng YL, Cheng PW, et al. Current mechanistic concepts in ischemia and reperfusion injury. *Cell Physiol Biochem*. 2018;46(4):1650–67.
69. Kalogeris T, Baines CP, Krenz M, Korthuis RJ. Cell biology of ischemia/reperfusion injury. *Int RevCell Mol Biol*. 2012;298:229–317.
70. Cutting KF. Wound exudate: composition and functions. *Br J Community Nurs*. 2003;8(9 Suppl):suppl 4–9.
71. Deskins DL, Ardestani S, Young PP. The polyvinyl alcohol sponge model implantation. *J Vis Exp*. 2012;(62):3885.
72. Efron DT, Barbul A. Subcutaneous sponge models. *Methods Mol Med*. 2003;78:83–93.
73. Alfaro MP, Deskins DL, Wallus M, DasGupta J, Davidson JM, Nanney LB, et al. A physiological role for connective tissue growth factor in early wound healing. *Lab Invest*. 2013;93(1):81–95.
74. Lim NS, Sham A, Chee SM, Chan C, Raghunath M. Combination of ciclopirox olamine and sphingosine-1-phosphate as granulation enhancer in diabetic wounds. *Wound Repair Regen*. 2016;24(5):795–809.
75. Stroncek JD, Reichert WM. Overview of wound healing in different tissue types. In: Reichert WM, editor. *Indwelling neural implants: strategies for contending with the in vivo environment*. Frontiers in neuroengineering. Boca Raton: 2008. Chapter 1. Available from: <https://www.ncbi.nlm.nih.gov/books/NBK3938/>.
76. Dunn RM, Huff W, Mancoll J. The rat rectus abdominis myocutaneous flap: a true myocutaneous flap model. *Ann Plast Surg*. 1993;31(4):352–7.
77. Merdan S, Mehmet B. Experimental Rat Flap Models. In: Sherif A, editor. *Issues in Flap Surgery*. Rijeka: IntechOpen; 2017. p. Ch2.
78. Ho BT, Weinberg H, Zhang WX, Aviv JE, Biller HF, Urken ML. Hemodynamics of the rodent abdominal skin flap following primary ischemia. *Laryngoscope*. 1993;103(9):981–4.
79. Zuber TJ. The mattress sutures: vertical, horizontal, and corner stitch. *Am Fam Physician*. 2002;66(12):2231–6.
80. McFarlane RM, Deyoung G, Henry RA. The design of a pedicle flap in the rat to study necrosis and its prevention. *Plast Reconstr Surg*. 1965;35:177–82.
81. Wada H, Vargas CR, Angelo J, Faulkner-Jones B, Paul MA, Ho OA, et al. Accurate prediction of tissue viability at postoperative day 7 using only two intraoperative subsecond near-infrared fluorescence images. *Plast Reconstr Surg*. 2017;139(2):354–63.
82. Hammond DC, Brooksher RD, Mann RJ, Beernink JH. The dorsal skin-flap model in the rat: factors influencing survival. *Plast Reconstr Surg*. 1993;91(2):316–21.
83. Martignago CCS, Tim CR, Assis L, Neves LMG, Bossini PS, Renno AC, et al. Comparison of two different laser photobiomodulation protocols on the viability of random skin flap in rats. *Lasers Med Sci*. 2019;34(5):1041–7.
84. Harder Y, Amon M, Erni D, Menger MD. Evolution of ischemic tissue injury in a random pattern flap: a new mouse model using intravital microscopy. *J Surg Res*. 2004;121(2):197–205.
85. Gupta A, Kumar P. Assessment of the histological state of the healing wound. *Plast Aesthetic Res*. 2015;2(5):239–42.
86. Datta S, Malhotra L, Dickerson R, Chaffee S, Sen CK, Roy S. Laser capture microdissection: Big data from small samples. *Histol Histopathol*. 2015;30(11):1255–69.
87. Tsuji JM, Whitney JD, Tolentino EJ, Perrin ME, Swanson PE. Evaluation of cellular wound healing using flow cytometry and expanded polytetrafluoroethylene implants. *Wound Repair Regen*. 2010;18(3):335–40.
88. Mahmood T, Yang PC. Western blot: technique, theory, and trouble shooting. *N Am J Med Sci*. 2012;4(9):429–34.
89. Aksamitiene E, Hoek JB, Kiyatkin A. Multistrip Western blotting: a tool for comparative quantitative analysis of multiple proteins. *Methods Mol Biol*. 2015;1312:197–226.
90. Liu CG, Calin GA, Volinia S, Croce CM. MicroRNA expression profiling using microarrays. *Nat Protoc*. 2008;3(4):563–78.
91. Bumgarner R. Overview of DNA microarrays: types, applications, and their future. *Curr Protoc Mol Biol*. 2013;Chapter 22:Unit 22.1.
92. Schmittgen TD, Livak KJ. Analyzing real-time PCR data by the comparative C(T) method. *Nat Protoc*. 2008;3(6):1101–8.
93. McDonald JH. *Local flaps in facial reconstruction*. 3rd ed. Baltimore: Sparky House Publishing; 2014.
94. Rada CC, Mejia-Pena H, Grimsey NJ, Canto Cordova I, Olson J, Wozniak JM, et al. Heat shock protein 27 activity is linked to endothelial barrier recovery after proinflammatory GPCR-induced disruption. *Sci Signal*. 2021;14(698):eabc1044.
95. Khanna S, Biswas S, Shang Y, Collard E, Azad A, Kauh C, et al. Macrophage dysfunction impairs resolution of inflammation in the wounds of diabetic mice. *PLoS One*. 2010;5(3):e9539.
96. Toth M, Sohail A, Fridman R. Assessment of gelatinases (MMP-2 and MMP-9) by gelatin zymography. *Methods Mol Biol*. 2012;878:121–35.
97. Blalock TD, Varela JC, Gowda S, Tang Y, Chen C, Mast BA, et al. Ischemic skin wound healing models in rats. *Wounds*. 2001;13(1):35–44.
98. Gibson DJ, Schultz GS. Molecular wound assessments: matrix metalloproteinases. *Adv Wound Care (New Rochelle)*. 2013;2(1):18–23.
99. McCarty SM, Percival SL. Proteases and delayed wound healing. *Adv Wound Care (New Rochelle)*. 2013;2(8):438–47.
100. Wong VW, Crawford JD. Vasculogenic cytokines in wound healing. *Biomed Res Int*. 2013;2013:190486.
101. Werner S, Grose R. Regulation of wound healing by growth factors and cytokines. *Physiol Rev*. 2003;83(3):835–70.
102. Lubkowska A, Dolegowska B, Banfi G. Growth factor content in PRP and their applicability in medicine. *J Biol Regul Homeost Agents*. 2012;26(2 Suppl 1):35–22S.
103. Maiese K, Boniece I, DeMeo D, Wagner JA. Peptide growth factors protect against ischemia in culture by preventing nitric oxide toxicity. *J Neurosci*. 1993;13(7):3034–40.
104. Kitta K, Day RM, Ikeda T, Suzuki YJ. Hepatocyte growth factor protects cardiac myocytes against oxidative stress-induced apoptosis. *Free Radic Biol Med*. 2001;31(7):902–10.
105. Planavila A, Redondo-Angulo I, Ribas F, Garrabou G, Casademont J, Giralt M, et al. Fibroblast growth factor 21 protects the heart from oxidative stress. *Cardiovasc Res*. 2015;106(1):19–31.
106. Zheng L, Ishii Y, Tokunaga A, Hamashima T, Shen J, Zhao QL, et al. Neuroprotective effects of PDGF against oxidative stress and the signaling pathway involved. *J Neurosci Res*. 2010;88(6):1273–84.
107. Humphrey RG, Sonnenberg-Hirche C, Smith SD, Hu C, Barton A, Sadovsky Y, et al. Epidermal growth factor abrogates hypoxia-induced apoptosis in cultured human trophoblasts through phosphorylation of BAD Serine 112. *Endocrinology*. 2008;149(5):2131–7.
108. Alsousou J, Thompson M, Hulley P, Noble A, Willett K. The biology of platelet-rich plasma and its application in trauma and orthopaedic surgery: a review of the literature. *J Bone Joint Surg Br*. 2009;91(8):987–96.
109. Kuffler DP. Variables affecting the potential efficacy of PRP in providing chronic pain relief. *J Pain Res*. 2019;12:109–16.
110. Cavallo C, Roffi A, Grigolo B, Mariani E, Pratelli L, Merli G, et al. Platelet-rich plasma: the choice of activation method affects the release of bioactive molecules. *BioMed Res Int*. 2016;2016:7.
111. Mohammadi R, Mehrdash M, Hassani N, Hassanpour A. Effect of platelet rich plasma combined with chitosan biodegradable film on full-thickness wound healing in rat model. *Bull Emerg Trauma*. 2016;4(1):29–37.
112. Law JX, Chowdhury SR, Saim AB, Idrus RBH. Platelet-rich plasma with keratinocytes and fibroblasts enhance healing of full-thickness wounds. *J Tissue Viability*. 2017;26(3):208–15.
113. Tambella AM, Attili AR, Dupre G, Cantalamessa A, Martin S, Cuteri V, et al. Platelet-rich plasma to treat experimentally-induced skin wounds in animals: a systematic review and meta-analysis. *PLoS One*. 2018;13(1):e0191093.
114. Wang B, Geng Q, Hu J, Shao J, Ruan J, Zheng J. Platelet-rich plasma reduces skin flap inflammatory cells infiltration and improves survival rates through induction of angiogenesis: an experiment in rabbits. *J Plast Surg Hand Surg*. 2016;50(4):239–45.
115. Li W, Enomoto M, Ukegawa M, Hirai T, Sotome S, Wakabayashi Y, et al. Subcutaneous injections of platelet-rich plasma into skin flaps modulate proangiogenic gene expression and improve survival rates. *Plast Reconstr Surg*. 2012;129(4):858–66.
116. Kim HY, Park JH, Han YS, Kim H. The effect of platelet-rich plasma on flap survival in random extension of an axial pattern flap in rabbits. *Plast Reconstr Surg*. 2013;132(1):85–92.
117. Tsai HC, Lehman CW, Chen CM. Use of platelet-rich plasma and platelet-derived patches to treat chronic wounds. *J Wound Care*. 2019;28(1):15–21.

118. Del Pino-Sedeño T, Trujillo-Martín MM, Andía I, Aragón-Sánchez J, Herrera-Ramos E, Iruzubieta Barragán FJ, Serrano-Aguilar P. Platelet-rich plasma for the treatment of diabetic foot ulcers: A meta-analysis. *Wound Repair Regen*. 2019;27(2):170–82.
119. Dauer DJ, Ferraro B, Song L, Yu B, Mora L, Buettner R, et al. Stat3 regulates genes common to both wound healing and cancer. *Oncogene*. 2005;24(21):3397–408.
120. Mattagajasingh SN, Yang XP, Irani K, Mattagajasingh I, Becker LC. Activation of Stat3 in endothelial cells following hypoxia-reoxygenation is mediated by Rac1 and protein Kinase C. *Biochim Biophys Acta*. 2012;1823(5):997–1006.
121. Sano S, Itami S, Takeda K, Tarutani M, Yamaguchi Y, Miura H, et al. Keratinocyte-specific ablation of Stat3 exhibits impaired skin remodeling, but does not affect skin morphogenesis. *EMBO J*. 1999;18(17):4657–68.
122. Chen SH, Murphy DA, Lassoued W, Thurston G, Feldman MD, Lee WM. Activated STAT3 is a mediator and biomarker of VEGF endothelial activation. *Cancer Biol Ther*. 2008;7(12):1994–2003.
123. Zegeye MM, Lindkvist M, Falke K, Kumawat AK, Paramel G, Grenegard M, et al. Activation of the JAK/STAT3 and PI3K/AKT pathways are crucial for IL-6 trans-signaling-mediated pro-inflammatory response in human vascular endothelial cells. *Cell Commun Signal*. 2018;16(1):55.
124. Hamilton K, Wolfswinkel EM, Weathers WM, Xue AS, Hatfeg DA, Izadoodst S, et al. The delay phenomenon: a compilation of knowledge across specialties. *Craniofacial Trauma Reconstr*. 2014;7(2):112–8.
125. Mukherjee P, Roy S, Ghosh D, Nandi SK. Role of animal models in biomedical research: a review. *Lab Anim Res*. 2022;38(1):18.
126. Robinson NB, Krieger K, Khan FM, Huffman W, Chang M, Naik A, et al. The current state of animal models in research: A review. *Int J Surg*. 2019;72:9–13.
127. Botting JH, Morrison AR. Animal research is vital to medicine. *Scientific American*. 1997;276(2):83–5.
128. Dominguez-Oliva A, Hernandez-Avalos I, Martinez-Burnes J, Olmos-Hernandez A, Verdusco-Mendoza A, Mota-Rojas D. The importance of animal models in biomedical research: current insights and applications. *Animals (Basel)*. 2023;13(7).
129. Ribitsch I, Baptista PM, Lange-Consiglio A, Melotti L, Patruno M, Jenner F, et al. Large animal models in regenerative medicine and tissue engineering: to do or not to do. *Front Bioeng Biotechnol*. 2020;8:972.
130. Mak IW, Evaniew N, Ghert M. Lost in translation: animal models and clinical trials in cancer treatment. *Am J Transl Res*. 2014;6(2):114–8.
131. Ruan Y, Robinson NB, Khan FM, Hameed I, Rahouma M, Naik A, et al. The translation of surgical animal models to human clinical research: A cross-sectional study. *Int J Surg*. 2020;77:25–9.
132. Bhuvanakrishna T, Wakefield S. A commentary on "The translation of surgical animal models to human clinical research: A cross-sectional study". *Int J Surg*. 2020;78:17–8.
133. Matthews RA. Medical progress depends on animal models - doesn't it? *J R Soc Med*. 2008;101(2):95–8.
134. Smith R. Animal research: the need for a middle ground. *BMJ*. 2001;322(7281):248–9.
135. Kelly RR, McCrackin MA, Russell DL, Leddy LR, Cray JJ, Larue AC. Teaching surgical model development in research by using situated learning and instructional scaffolding. *J Am Assoc Lab Anim Sci*. 2019;58(3):321–8.
136. Masunaga T, Kato M, Sasaki M, Iwata K, Miyazaki K, Kubosawa Y, et al. Novel quantitative assessment indicators for efficiency and precision of endoscopic submucosal dissection in animal training models by analyzing an electrical surgical unit. *Dig Endosc*. 2023.
137. Kehinde EO. They see a rat, we seek a cure for diseases: the current status of animal experimentation in medical practice. *Med Princ Pract*. 2013;22(Suppl 1):52–61.
138. Bergmeister KD, Aman M, Kramer A, Schenck TL, Riedl O, Daeschler SC, et al. Simulating surgical skills in animals: systematic review, costs & acceptance analyses. *Front Vet Sci*. 2020;7.
139. Rhodin KE, Leraas HJ, Tracy E, Sudan R, Migaly J. A Role for live-animal models in undergraduate surgical education during the Cadaver shortage. *Ann Surg Open*. 2023;4(2):e274.
140. Drysch M, Wallner C, Schmidt SV, Reinkemeier F, Wagner JM, Lehnhardt M, et al. An optimized low-pressure tourniquet murine hind limb ischemia reperfusion model: inducing acute ischemia reperfusion injury in C57BL/6 wild type mice. *PLOS ONE*. 2019;14(1):e0210961.
141. Bergmeister KD, Aman M, Kramer A, Schenck TL, Riedl O, Daeschler SC, et al. Simulating surgical skills in animals: systematic review, costs & acceptance analyses. *Front Vet Sci*. 2020;7:570852.
142. Loh CYY, Wang AYL, Tiong VTY, Athanassopoulos T, Loh M, Lim P, et al. Animal models in plastic and reconstructive surgery simulation—a review. *J Surg Res*. 2018;221:232–45.
143. Ozcan G, Shenaq S, Spira M. A new flap model in the rat. *Ann Plastic Surg*. 1991;27(4):332–8.
144. Machens HG, Morgan JR, Berthiaume F, Stefanovich P, Reimer R, Berger AC. Genetically modified fibroblasts induce angiogenesis in the rat epigastric island flap. *Langenbecks Arch Surg*. 1998;383(5):345–50.
145. Erni D, Sakai H, Banic A, Tschopp HM, Intaglietta M. Quantitative assessment of microhemodynamics in ischemic skin flap tissue by intravital microscopy. *Ann Plast Surg*. 1999;43(4):405–14. Discussion 14–5.
146. Sonmezoglu S, Fineman JR, Maltepe E, Maharbiz MM. Monitoring deep-tissue oxygenation with a millimeter-scale ultrasonic implant. *Nat Biotechnol*. 2021;39(7):855–64.
147. Hoang Nguyen T, Kloeppel M, Hoehnke C, Staudenmaier R. Influence of silicone sheets on microvascular anastomosis. *Clin Orthop Relat Res*. 2008;466(12):3123–9.
148. Jeong HS, Lee HK, Tark KC, Lew DH, Koh YW, Kim CH, et al. Effect of endogenous bone marrow derived stem cells induced by AMD-3100 on expanded ischemic flap. *J Korean Med Sci*. 2014;29(Suppl 3):S237–48.
149. Jones M, Zhang F, Blain B, Guo M, Cui D, Dorsett-Martin W, et al. Influence of recipient-bed isolation on survival rates of skin-flap transfer in rats. *J Reconstr Microsurg*. 2001;17(8):653–8. Discussion 9.
150. Heimer S, Schaefer A, Mueller W, Lass U, Gebhard MM, Germann G, et al. Bed isolation in experimental flap studies in rats: a dispensable procedure. *Ann Plast Surg*. 2013;70(3):354–9.
151. Davidson JM, Yu F, Opalenik SR. Splinting strategies to overcome confounding wound contraction in experimental animal models. *Adv Wound Care (New Rochelle)*. 2013;2(4):142–8.
152. McFarlane RM, Heagy FC, Radin S, Aust JC, Wermuth RE. A study of the delay phenomenon in experimental pedicle flaps. *Plast Reconstr Surg*. 1965;35:245–62.
153. Liu HL. Microvascular anastomosis of submillimeter vessels—a training model in rats. *J Hand Microsurg*. 2013;5(1):14–7.
154. Ozkan O, Koshima I, Gonda K. A supermicrosurgical flap model in the rat: a free true abdominal perforator flap with a short pedicle. *Plast Reconstr Surg*. 2006;117(2):479–85.
155. Mofikoya BO, Ugburo AO, Bankole OB. Microvascular anastomosis of vessels less than 0.5 mm in diameter: a supermicrosurgery training model in lagos, Nigeria. *J Hand Microsurg*. 2011;3(1):15–7.
156. Lim SY, Yeo MS, Nicoli F, Ciudad P, Constantinides J, Kiranantawat K, et al. End-to-patch anastomosis for microvascular transfer of free flaps with small pedicle. *J Plast Reconstr Aesthet Surg*. 2015;68(4):559–64.
157. Casal D, Pais D, Iria I, Mota-Silva E, Almeida MA, Alves S, Pen C, Farinho A, Mascarenhas-Lemos L, Ferreira-Silva J, Ferraz-Oliveira M, Vassilenko V, Videira PA, Gory O'Neill J. A model of free tissue transfer: The rat epigastric free flap. *J Vis Exp*. 2017;(119):55281.
158. Ren Z, Cui S, Lyu S, Wang J, Zhou L, Jia Y, et al. Establishment of rat allogenic vein replacement model and pathological characteristics of the replaced vessels. *Front Surg*. 2022;9:984959.

Publisher's Note

Springer Nature remains neutral with regard to jurisdictional claims in published maps and institutional affiliations.